EFFECTS OF GEOMETRICAL UNCERTAINTIES IN A GAS COOLED FAST REACTOR

C.M.H. Hartman

Bachelor Thesis
PNR-131-2012-001

Supervisors:
Z. Perkó
dr. ir. J.L. Kloosterman

Delft University of Technology
Faculty of Applied Sciences
Department of Radiation Radionuclides & Reactors
Section of Physics of Nuclear Reactors

January 11, 2012

Abstract

In this research project the geometrical uncertainties in a Gas Cooled Fast Reactor were investigated. The work focused on the imprecisions found in the fuel pins and the fuel assemblies, which can arise from production tolerances of the individual volumes of the fuel pin or those of the grid used to position the fuel pins in the assembly.

The SCALE modules XSDRN and NEWT were used to simulate a fuel pin in an infinite array of fuel pins and a fuel assembly in an infinite array of fuel assemblies respectively. The individual effects of different geometrical uncertainties in both the former and the latter case were examined on the output parameter k_{eff}, and for most uncertain parameters a Gaussian distribution was assumed. For the fuel pin combined effects were also researched.

An in-house made thermal-hydraulics code was also used together with XSDRN to calculate the temperature and power density profile in a fuel pin. This made it possible to study the correlation between geometrical uncertainties and several thermal-hydraulic parameters.

The uncertainty in the fuel pellet radius has the biggest effect on the k_{eff}, as it introduces an uncertainty of 0.17% in this output parameter. This effect is solely due to uncertainty in the fuel mass, with the density assumed constant. The rhenium liner also has a significant effect on the neutronics of the reactor, introducing an uncertainty of 0.15%. The tungsten-rhenium liner and the cladding contribute less to the uncertainty. Fuel pellet movement inside the pin and fuel pin displacement have no or very little effect on the neutronics.

Uncertainty in the fuel pellet radius and cladding width are the main contributors to the uncertainty in thermal parameters. The cladding introduces a uncertainty of 0.08% in the various temperatures, increasing both the average and maximum temperatures in every part of the pin. The only contributor to uncertainty in the power density profile is the uncertainty in the fuel pellet radius, introducing a uncertainty of 0.58%.

Contents

List of Tables

List of Figures

Chapter 1

Introduction

1.1 Aim of this research project

In this research project the uncertainties arising from geometrical imprecisions in a Gas Cooled Fast Reactor were investigated. These geometrical errors can be found in every part of the reactor, but the most important ones are those present in the fuel pins and the fuel assemblies. The imprecisions in the pins include the radius of the fuel pellets coming from the uncertainty of the fuel mass or density and the thickness of the liners and the cladding. The geometrical uncertainties in the fuel assemblies are due to the displacement of the fuel pellets inside the pins or the uncertainty in the position of the pins within the fuel assemblies.

In this project these geometrical errors were modeled and their contribution to the uncertainty of certain performance parameters, such as the effective multiplication factor k_{eff} or the temperature in different parts of the pin was determined.

1.2 Outline of this thesis

In the first chapter the Gas Cooled Fast Reactor and its most relevant characteristics are detailed, with special attention to the main focus of this research, the fuel pin and fuel assembly. The second chapter provides a brief introduction to uncertainty analysis and the direct Monte Carlo method, including some remarks on the probability distributions and the sampling techniques used. The theory ends with a very short overview of the neutron transport equation and the discretization necessary in order to solve it. In chapter 3, XSDRN and NEWT, two modules of the reactor physics program SCALE are introduced, which were used to build a simplified model of a GFR. Results are presented in chapter 4 in three parts, first an overview of the results for the 1D model is given,

followed by those of the 2D model and the thermal-hydraulic calculations. The thesis ends with conclusions and some recommendations for future work.

1.3 Generation IV initiative

The increasing world population is expected to increase its electricity consumption substantially over the next decades [5]. Ideally this electricity would be supplied by sources which are safe, clean and have only a modest impact on the environment. With the increasing fear of the effects of greenhouse gas emission, eyes are turned to nuclear power. Already a fair share of the world's electricity is being produced by nuclear power plants, however they all share the major drawback of producing nuclear waste, which needs to be stored safely for thousands of years. Some recycling of this waste is already being done at the moment, but a closed fuel cycle, which would solve a lot of issues, is still far from reach. In order to bring nuclear power to the 21^{st} century and hundreds of years to come, countries worldwide have combined their research efforts in the Generation IV technological roadmap [13]. This initiative lays out a framework for the necessary steps to be taken to build a new generation of innovative nuclear systems, which are characterized by competitive economics, sustainability, safety and proliferation resistance.

One of the six Generation IV reactor concepts is the Gas Cooled Fast Reactor (GFR). This reactor features a closed nuclear fuel cycle and makes use of a fast neutron spectrum, enabling the fission of not only fissile materials such as ^{235}U and ^{239}Pu, but also that of fissionable isotopes such as ^{238}U, which makes up more than 99 percent of the world's natural uranium resources. The hard neutron spectrum enhances the conversion of ^{238}U to ^{239}Pu compared to thermal reactors, allowing the GFR to be used for breeding. Moreover, its fast spectrum enables the burning of long lived minor actinides, greatly reducing their environmental hazard and considerably improving the GFRs sustainability aspects.

The GFR, being a fast reactor, has no moderator and has a more compact core than a thermal reactor. It is cooled with low density helium pressurized at 60 bar, providing a number of advantages: no phase change occurs in the core that would impose limitations on the outlet temperature, the coolant does not react with other materials and it absorbs no neutrons. The higher core outlet temperature should make it possible to reach an efficiency of 45%. Naturally the concept has disadvantages as well: due to the lack of moderator and the fast neutron spectrum, some of the safety parameters are less favourable, for example both the effective delayed neutron fraction and the neutron generation time is smaller than in thermal reactors, decreasing the grace time.

1.4 The GFR2400 model

1.4.1 Fuel pin design

The typical coolant temperatures in a GFR core range from 400 to 900°C, while typical fuel temperatures can rise up to 1400°C. In order to withstand such high temperatures, together with high radiation and high neutron flux in the core, new types of fuel pins have to be designed. Metals used in thermal reactors, such as zircaloy, have a too low melting point and cannot serve as cladding, nor seems to be the traditional oxide fuel applicable in the GFR.

In the European GFR2400 design, which was the base of this research, ceramics (SiC) are considered as main component for the cladding, sealed with a SiC liner on the outside. Ceramics have the advantage that they preserve mechanical properties at higher temperatures and show little sensitivity to oxidation in this temperature range. However material tests have proven [14] that ceramics cannot ensure leak-tightness against fission products by themselves and thus a refractory liner on the inside is required.

These liners must be chosen carefully, as it is well known that refractory metals can have a high neutron capture cross section and have an impact on the neutronics of the reactor. After careful consideration a double liner has been chosen for GFR2400, first a tungsten-rhenium alloy of 40 μm and second a pure rhenium liner of 10 μm. The gap between the liners and the fuel pellet is filled with helium.

The fuel itself is a combination of plutonium carbide and uranium carbide. Carbide is preferred over the traditional oxide fuels mostly because of its high melting point, high density and high conductivity. The uranium carbide is made from natural uranium, that is with a 0.72% molar percentage of ^{235}U and 99.28% of ^{238}U. The isotopic composition of the plutonium is more diverse, the main components are ^{239}Pu (56.0%) and ^{240}Pu (25.9%), similar to the isotopic composition of plutonium in twice recycled MOX fuel, expected to be available from the nuclear reprocessing plants in France after 2016 [12].

1.4.2 Fuel pin production

Fuel pin manufacturing starts with the production of the ceramic tube. This can give production errors and imprecisions on both the outside and on the inside of the tube. Imprecisions on the outside of the tube have their effect on the distance between the fuel pin and its neighbours, which in turn determines the amount of coolant flowing in the different sub-channels. Imprecisions on the inside of the tube effect the size of the helium gap between the fuel pellet and the cladding. After the production of the tube, the liners are applied on the inside. Technological challenges regarding the production of these liners are the thickness of the layers and the length over which they have to be

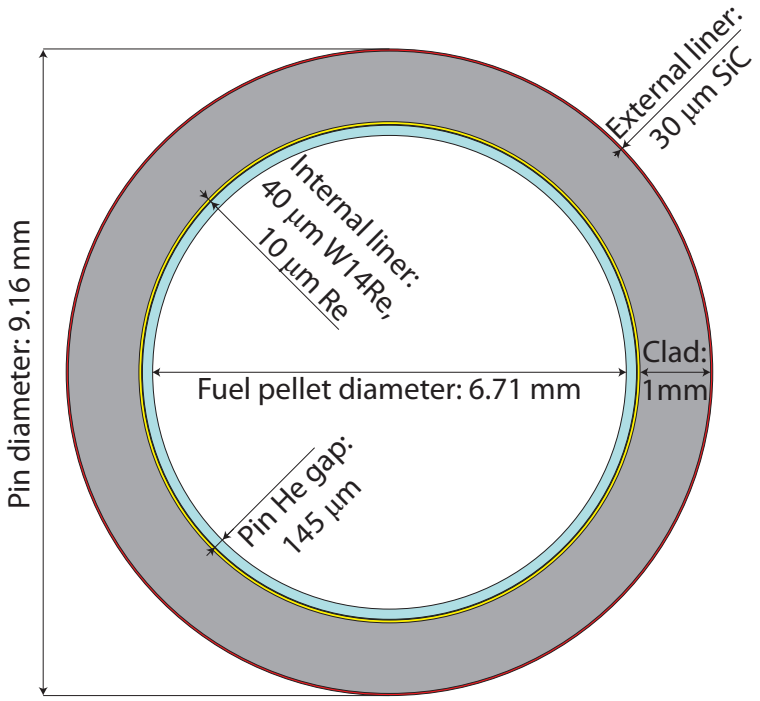

Figure 1.1: Schematic overview of a GFR2400 fuel pin [12]

applied. Imprecisions in the thickness of the liners also have their effect on the helium gap size, either decreasing or increasing it.

The production of fuel pellets is a better known process. Fuel pellets are pressed in a volume with a certain production tolerance. The size (radius and height) of the pellet can vary either due to the uncertainty in the fuel mass used for the production, with the density assumed to be precise, or due to the uncertainty in the density of the fuel, with the mass weighed beforehand and assumed precise. Usually the position of the fuel pellets within the pin, is also uncertain, as pellets can move freely.

1.4.3 Fuel assembly

The fuel assembly of GFR2400 consists of 217 fuel pins arranged in a hexagonal array. The whole fuel assembly is contained within a SiC wrapper of 2 mm width. The entire core contains 516 of these fuel assemblies. In the assembly the individual pins are positioned and secured with grids which can again only be produced with a certain tolerance level. Hence imprecisions are always present in the form of the position of the pins being different from the designated one.

In the GFR2400 design there are two types of fuel assemblies, one with a higher plutonium content for the outer, and one with a lower plutonium content for the inner region

of the core. In this research only the fuel assembly with lower plutonium content was investigated.

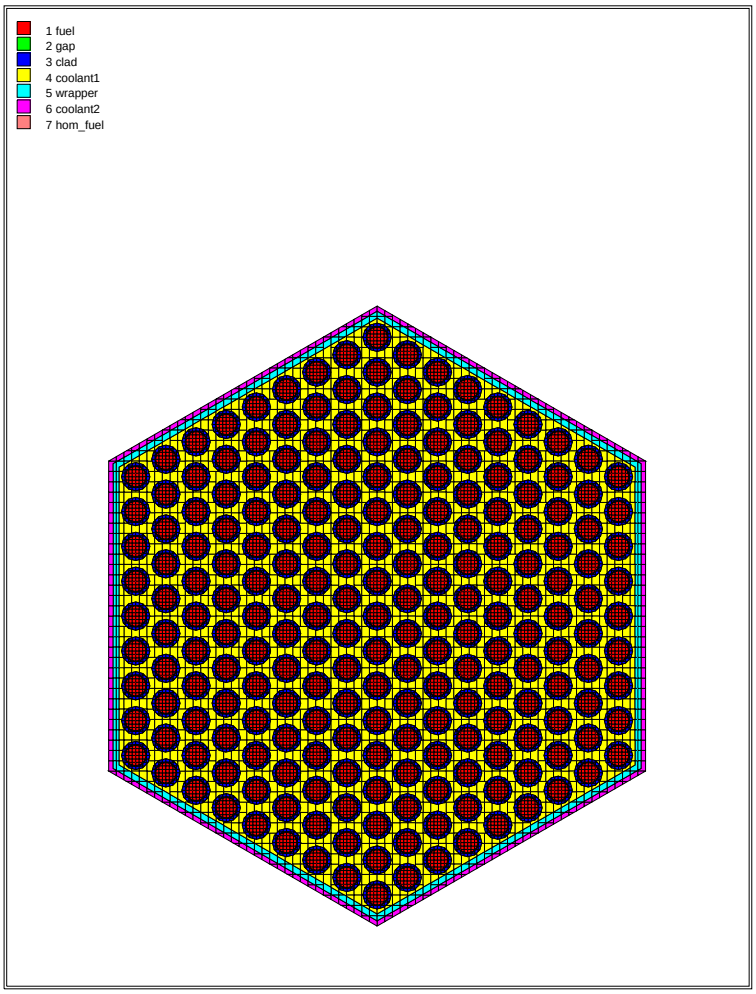

Figure 1.2: Schematic overview of a GFR2400 fuel assembly

Chapter 2

Theory

2.1 Uncertainty theory

Every measurement and mathematical model brings its own imprecisions with it. These have numerous causes: in an experiment there are always instrument errors present, manufacturing can only be done within certain tolerance levels, in a model there are simplifications or assumptions, numerical errors, etc.

In numerical simulations any input parameter can have an influence on the output of the model, hence any imprecision, or uncertainty, in that input parameter can have an effect on the uncertainty of the output. The role of uncertainty analysis is to make an evaluation of how the imprecision in the input parameters becomes apparent in the uncertainty of an output parameter of interest.

Most techniques used to perform uncertainty analysis are statistical methods. To be able to perform a statistical uncertainty analysis it is necessary to assign a range and a distribution function for each input parameter to be investigated. Uncertainties in output parameters are then for example characterized by estimates of the average value and the standard deviation. The method used in this research to obtain these is called the direct Monte Carlo method.

2.2 The direct Monte Carlo Method

Monte Carlo uncertainty analysis methods usually follow a certain pattern. First probability density functions (pdfs) with a given range are assigned to all possible input parameters. Then random sampling is used to generate a series of inputs, where the input parameters are distributed in accordance with their probability density function. The full model is then run with each input to produce a series of outputs. Finally, the parameters of interest in the output are evaluated.

2.2.1 Distributions

In the ideal case there would be experimental data available from which a probability density function could be determined for the different input parameters, in our case for the radii of the fuel pin components and for the positions in the fuel assembly. The design of the GFR2400 fuel pin and fuel assembly are however innovative new designs, in particular the long metal liners and the ceramic cladding form a technological challenge and experimental data is simply not available. As no experimental data could be used for the probability density functions, a Gaussian distribution was assumed which is considered as a good first approximation when the pdf of an uncertainty is unknown.

A Gaussian distribution is a function of the form

$$f(x) = \frac{1}{\sqrt{2\pi\sigma^2}} e^{-\frac{(x-\mu)^2}{2\sigma^2}} \tag{2.1}$$

In Formula 2.1 μ is the average or expected value of the parameter and σ^2 is the variance, which is a measure of the spread around the average value. The square root of the variance is called the standard deviation σ.

For almost every perturbation made in this research, a Gaussian distribution was assumed, with one exception: the fuel pellets can move freely within the pin and thus a uniform distribution was assumed in that case.

2.2.2 Choice of σ

Obviously the choice of the standard deviation σ is crucial for the range of input values allowed. For the radius of the fuel pellet a whole range of σ has been investigated between 1μm and 40μm. For both the metallic liners a standard deviation of 1μm was assumed. For the rhenium liner this is a σ of already 10 %, which might seem unreasonably high, however manufacturing tests should demonstrate whether at least such precision can be reached or not. It is possible to "grow" thin layers of metals, but to be able to do this over a length of over 1.5 m might still be a technological challenge. The production of ceramic tubes over this length is also difficult and thus a σ of 10 μm has been chosen as standard deviation, both inside and outside of the tube.

Table 2.1: Different σ's used for the different parts of the pin

Region	σ [μm]	% of radius/width
Fuel pin	1, 2, 3, 4, 5, 10, 15, 20, 25, 30, 33, 40	0.03, 0.06, 0.09, 0.12, 0.15, 0.30, 0.45, 0.60, 0.75, 0.89, 0.98, 1.19
W14-Re liner	1	2.5
Re liner	1	10
Cladding	10	0.97

2.2.3 Random sampling

A Gaussian distribution ranges from -∞ to +∞, but since 99.7% of the values lie within a $6 \cdot \sigma$ wide region, the range for possible values was restricted to $\mu \pm 3 \cdot \sigma$. Generating enough samples from the input parameters to obtain a proper data set for the output is always a trade-off between precision and computational time. Initial test were done with 100 and 250 data points, however this did not give a smooth enough result. For the rest of this research a data set of 1000 samples was considered sufficient as this did give enough data points to accurately evaluate the results, without exceeding acceptable computational time limits.

For sampling the Gaussian distributions of the input parameters multiple methods can be used. In this research the rejection sampling method was chosen, which is not the most efficient but is easy to code. In this technique first a random number ξ_1 is generated uniformly within the range of the parameter $(\mu \pm 3 \cdot \sigma)$. Then a second random number ξ_2 is generated between 0 and the maximum of the probability density function. For a Gaussian distribution this is the value of $\frac{1}{\sqrt{2\pi\sigma^2}}$, which is reached at $\xi = \mu$, the average value. When f(ξ_1) $< \xi_2$, the value ξ_1 is accepted as an input value. When this equation does not hold, the value ξ_1 is rejected and a new value for ξ_1 is chosen. This sampling is repeated until the appropriate number of input values is reached.

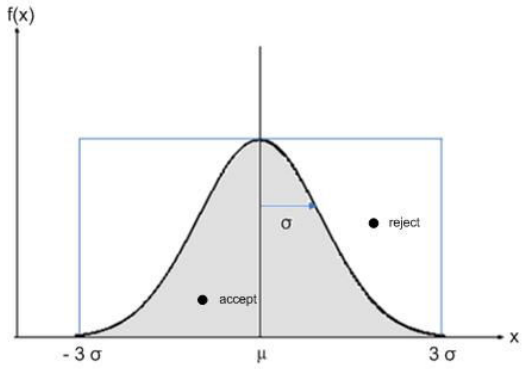

Figure 2.1: Rejection sampling [2]

2.3 Results analysis

As mentioned before, statistical methods were used to obtain a series of inputs. Statistical methods can also be used to examine the series of outputs produced. Because we were interested in the relative effect of the perturbations, the input and output parameters were normalized. The input parameters were converted to reflect the change in radius or width of a part of the fuel pin, the output parameters (e.g. k_{eff}) were converted to reflect the relative change from their mean value.

For each series of outputs, the shape of the distribution in the output parameter k_{eff} was analyzed. The key parameter of interest was the standard deviation of the output. This gives a good view of how the variation in the input causes a variation in the output.

Mappings of the uncertain inputs to the uncertain outputs were also made in the form of scatter plots. A convenient tool to analyze scatter plots is linear regression, where it is tried to model the data points in a linear function of the form $y = A + Bx$. The slope of the linear curve, B, gives information on how strongly the model (the output parameter being investigated) responds to the input parameter.

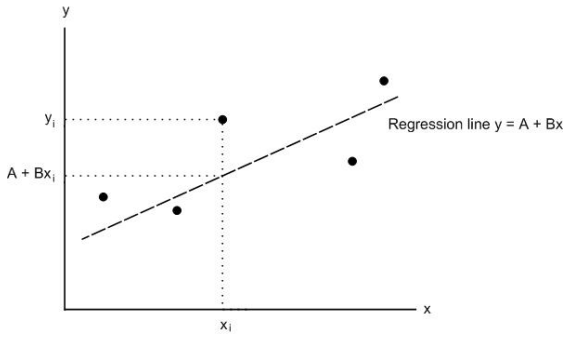

Figure 2.2: The least squares method minimizing the sum of the differences squared between the data point y_i at x_i and the value $A+Bx_i$ on the regression line $y = A+Bx$ [7]

In order to obtain this linear function, the least-squares method can be used. In the least-squares method the coefficients in the regression line are obtained by minimizing the squares of the distances between the data points and the regression line [11]. This gives

$$S(A, B) = \sum_{i=1}^{n} (y_i - (A + Bx_i))^2 \tag{2.2}$$

The quality of the linear regression performed is expressed in $\bar{R}^2$, which is a number between 0 and 1. The closer it is to 1, the better the regression line models the experimental data. It tells us how much of the variation can be explained by the model. This number is a useful tool to compare data sets where the output is not dependent on only one parameter, but two. The higher the $\bar{R}^2$, the more sensitive the output is to the certain input.

2.4 The neutron transport equation

The most important equation in nuclear reactor physics, from the neutronics point of view, is the Boltzmann neutron transport equation, which is an exact description of the

neutrons average behavior. The time-independent transport equation is given by

$$\hat{\Omega} \cdot \nabla \phi \left(\vec{r}, E, \hat{\Omega} \right) + \Sigma_t \left(\vec{r}, E \right) \phi \left(\vec{r}, E, \hat{\Omega} \right) = \int_{4\pi} d\hat{\Omega}' \int_0^{\infty} dE' \Sigma_s \left(\vec{r}, E' \rightarrow E, \hat{\Omega}' \rightarrow \hat{\Omega} \right) \phi \left(\vec{r}, E', \hat{\Omega}' \right) + S \left(\vec{r}, E, \hat{\Omega} \right) \quad (2.3)$$

This balance equation respectively states that neutron losses due to leakage and collisions must equal the scattering of neutrons and a source term, in some energy range dE about E, in a volume d^3r about $\vec{r}$ in direction $d\hat{\Omega}$ about solid angle $\hat{\Omega}$. In Formula 2.3 $\phi \left(\vec{r}, E, \hat{\Omega} \right)$ represent the flux at a certain point in the reactor, with a certain direction and energy. Σ_t represents the total cross section, Σ_s the scattering cross section and S $\left(\vec{r}, E, \hat{\Omega} \right)$ a source of neutrons with a certain energy, at a certain point with a certain direction. It is assumed that the reader is familiar with the basics of nuclear reactor physics. For a more detailed and complete derivation, the reader is referred to Duderstadt and Hamilton [6].

2.4.1 Discretization

The variables E, $\hat{\Omega}$, and $\vec{r}$ are continuous variables. In order to solve this equation numerically, these variables have to be discretized. The spatial variable $\vec{r}$ can be discretized by decomposing the space into small volumes with an appropriate mesh. Later in this chapter the specific meshes used in this research are given. The neutron energy E spans from 10^{-5} eV up to 10^7 eV and some of the processes, for example the fission cross section, depend quite sensitively on the neutron energy. During discretization the neutron energy is divided into energy groups, and specific methods are used to appropriately weight the continuous cross sections to calculate the group cross sections. Several libraries are available, in this research the 238 group ENDF/B-VII cross section library of SCALE was used.

In order to discretize the direction variable $\hat{\Omega}$, a few options are available, in the codes used in this research the discrete ordinate approach is used. In this method the independent variable $\hat{\Omega}$ is represented by a discrete set of directions $\hat{\Omega}_n$. Functions depending on $\hat{\Omega}$ are then only represented by their value at each of these discrete directions.

$$f \left(\hat{\Omega} \right) \rightarrow f \left(\hat{\Omega}_n \right) \equiv f_n, n = 1, \ldots, N \quad (2.4)$$

The integral over $\hat{\Omega}$ in the neutron transport equation becomes a summation over f_n with appropriately chosen quadrature weights w_n. When this discrete ordinates approach is used, the neutron transport equation reduces to a coupled set of N equations, also known

as the S_N equations. These equations have the form of

$$\hat{\Omega}_n \cdot \nabla \phi_n (\vec{r}, E) + \Sigma_t (\vec{r}, E) \phi_n (\vec{r}, E) = \sum_{n'=1}^{N} w_{n'} \int_0^{\infty} dE' \Sigma_s \left(\vec{r}, E' \to E, \hat{\Omega}_{n'} \to \hat{\Omega}_n \right) \phi_n \left(\vec{r}, E' \right) + S_n (\vec{r}, E)$$
$$n = 1, \ldots, N \text{ and } \phi_n (\vec{r}, E) = \phi \left(\vec{r}, E, \hat{\Omega}_n \right) \quad (2.5)$$

The S_N equations can be solved numerically by a computer. In the codes used during this research the angular quadrature was chosen to be S16. Experiments with higher quadrature orders have been done, but this only led to more computational time and not to more accurate results.

2.4.2 Output

From the S_N equations the flux in every volume element and energy group in a certain system can be calculated along with the effective neutron multiplication factor k_{eff}. This is the ratio of the rate of neutron production and the rate of neutron loss (absorption plus leakage) in a reactor. For $k_{eff} = 1$ on average every fission causes another fission and a chain reaction can be sustained, therefore the system is called critical. A system needs to be at least critical to be able to ever sustain a nuclear chain reaction. In practice reactors always operate at k_{eff} of 1. Values of k_{eff} calculated in this research are higher than 1, corresponding to a situation where the control rods are not inserted in the core, but are positioned above it.

In this research one of the prime subjects of investigation was the effect of geometrical variations in the system on the k_{eff}.

Chapter 3

Codes and methods

In numerical simulations regarding reactor physics SCALE is often used. SCALE stands for Standardized Computer Analyses for Licensing Evaluation and was developed by the Oak Ridge National Laboratory for the U.S. Nuclear Regulatory Commission and U.S. Department of Energy with the aim to develop a complete simulation package to perform standardized nuclear safety analysis and reactor design testing [10]. It is used worldwide to research and model the neutronics aspect of nuclear systems. SCALE is built up in modules, which all have their own characteristics and are used for different purposes. For this research two SCALE modules were used for the transport calculations (and several smaller ones for auxiliary tasks).

In this chapter an overview of these codes is given together with details on how the specific calculations were performed. A finite difference thermal-hydraulics code was also used in order to calculate temperature and power density profiles, a short introduction to this code and its most important characteristics is also included.

3.1 XSDRN

XSDRN is a module within SCALE that can solve the one-dimensional Boltzmann neutron transport equation using the discrete ordinates approach [9]. As an output it gives among other things the fluxes in every interval specified and the effective multiplication factor k_{eff}. This module was used to perform calculations on a single fuel pin of GFR2400 in an infinite array of pins. This is a simple and rather crude approximation of the reactor core, but is easy and fast to calculate.

The fuel pin was modeled as a series of cylinders inside one another. The outside SiC liner was modeled as being one with the SiC cladding, which reduces computational time without affecting results. The cylindrical symmetry allows us to handle the problem as 1 dimensional. The axial axis was considered with a buckling and the boundary conditions

were chosen in a way to simulate the individual pin in an infinite array of fuel pins. As mentioned before, the 238 group ENDF/B-VII cross section library was used.

The fuel pin was divided into 36 spatial (radial) intervals, not necessarily equally spaced. The more interesting regions were divided into more intervals. The fuel is by far the most interesting region as it is the region with the highest neutron flux. Increasing the number of intervals above 36 did not affect the results and only increased computational time. In Table 3.1 an overview of the dimensions of the fuel pin is given together with the distribution of the intervals.

Table 3.1: Dimensions of the different materials with the number of intervals used

Region	Radius [cm]	Width [cm]	Intervals
Fuel pin	0.3355	0.710	18
Helium gap	0.35	0.0145	1
W14-Re liner	0.354	0.004	1
Re liner	0.355	0.001	1
Cladding (with SiC liner)	0.458	0.103	6
Coolant	0.5785	0.1205	9

The first part of this research focused on the effects of geometrical uncertainties in the fuel pin, which means the uncertainties in the radii of the different parts of the pin. First, the effects of perturbing the individual radii independently were investigated. The following radii were perturbed, all following a Gaussian distribution with their own standard deviation to see their individual effect: fuel pellet radius, tungsten-rhenium liner, rhenium liner, cladding on the inside - all at the expense of the helium gap - and finally, cladding on the outside at the expense of the coolant. Second all possible combinations were made to see the combined effect and to determine which effect is stronger, or in other words, to what input parameter the output parameter is more sensitive to. Last, for completeness, every radius was perturbed at the same time to see the overall effect.

XSDRN is also capable of using the calculated fluxes to calculate new input cross sections. This can for example be used when parts of the geometry have to be homogenized. In this research this was needed in order to simulate the displacement of the pellets inside the fuel pin and that of the fuel pins in the assembly using 2D transport calculations. For the former, the liners were homogenized with the cladding, as these intervals are simply too small in the big model and can only add more computational time, without adding interesting results. This homogenization introduced an error of 16 pcm (one one-thousandth of a percent or 10^{-5}) which is acceptable. In order to model the effect of the pin displacements in the assembly the pins also had to be completely homogenized (this was needed for collapsing the cross sections of the surrounding SiC wrapper correctly). This introduced an error of 1 pcm, which is negligible.

3.2 NEWT

NEWT is a module within SCALE that can solve the two-dimensional neutron transport equation and is able to handle models with complex 2 dimensional geometries [4], such as a fuel assembly. Unfortunately, circular geometries cannot be handled by NEWT precisely, hence the cladding and fuel pin were modelled as 12 sided hexagons, where the volume of the components was preserved. As mentioned before, the cladding and liners were modelled as one homogenized material.

The second part of this research focused on the effects of uncertainty in the position of the fuel pellets inside the cladding and the uncertainty in the position of the fuel pins within the grid of the fuel assembly. For the first, all fuel pellets were positioned inside the cladding using a uniform distribution, keeping in mind that the displacement is bounded by the inside of the cladding. For the uncertainty in the position of the fuel pins within the grid, all fuel pin positions were perturbed following a Gaussian distribution at the same time. This was done for several standard deviations having the value 1 μm, 10 μm, 100 μm and 400 μm.

3.2.1 Input for NEWT

To produce an acceptable 2D NEWT model of the fuel assembly, the following scheme, depicted in Figure 3.1 was used, containing several SCALE modules.

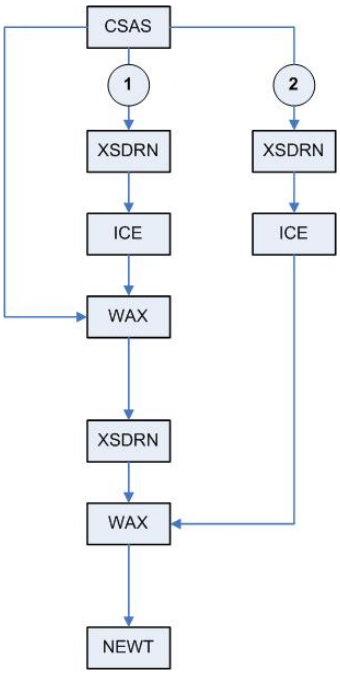

Figure 3.1: Input scheme for NEWT

CSAS is a module within SCALE that produces a problem-dependent macroscopic cross section library, in this case a 238 group library. ICE is a module that can mix multigroup cross sections and was used in this calculation scheme to produce homogenized macroscopic cross sections. WAX is a module that can merge different cross section libraries together and was used to merge the cross sections coming from different routes.

In the first path first (on the left in Figure 3.1) a fuel pin and the surrounding coolant is homogenized in 238 groups with XSDRN. This homogenized cross section is then filled into the fuel assembly in a second XSDRN model to correctly take into account the outside SiC wrapper and helium. This XSDRN run also collapses the cross section into 20 groups. The result of this first path is the collapsed 20 groups cross section of the fuel assembly wrapper and the outside coolant. The second path (on the right) homogenizes the metallic liners with the cladding and collapses the cross sections into 20 groups. The final WAX module merges the two paths, producing a 20 group cross section library with all the materials present. The NEWT input hence consists of one fuel assembly surrounded by a SiC wrapper and coolant, but with 217 individual pins with the cladding and liners homogenized.

3.2.2 Group collapsing

The initial calculations showed that using a 238 group energy discretization in the 2D transport calculations takes too much computational time. Hence it was decided to collapse the 238 energy groups into 20 groups. Around 30 combinations were tried, but it proved to be impossible to figure out a perfect combination giving identical results to the 238 group calculations. Some attempts were done with collapsing into 44 groups, but this did not give better results than the 20 group library. The group collapsing finally used introduced an error of 73 pcm in the k_{eff}. However, since the main concern of this research was the relative variation, further efforts to get closer to the original value were abandoned.

3.3 Thermal hydraulics model

The last part of this research focused on the effect of an uncertain radius on the temperature profile and the power density in the pin. XSDRN was used together with an in-house made thermal-hydraulics code specifically designed to calculate the temperature profile in the pin of GFR2400. The program is a finite difference code that solves the heat transfer equations in steady state for the fuel pin of GFR2400. It takes into account non-linearities due to the temperature dependence of thermal-hydraulic parameters such as heat conductance.

For one input XSDRN was used twice: first it was run with one perturbed radius in cylindrical geometry to create a radial flux profile (36 intervals), second it was run with

a slab geometry to create an axial flux profile (500 intervals). The reflectors, plenums and control mechanism (supposed to rest in the upper plenum above the core) were taken into account in this model.

The program then uses the power density profile of the pin as the heat source, which is gained by combining the axial and radial flux profiles into a virtual 3D (R-Z) profile, and calculates the temperature profile for the pin.

Each radius was perturbed following the same Gaussian distributions as before and for each perturbation the average and maximum temperature in different parts of the fuel pin, plus the power peaking factor were calculated, to determine the effects of geometrical uncertainties on these quantities.

Chapter 4

Results

In this chapter the most important outcome from the research are given, divided into two parts. First the neutronics and second the thermal-hydraulic results are given.

4.1 Neutronics

The neutronics results are divided in several sections. First those from the 1D calculations are presented (Sections 4.1.1-4.1.2), showing the effects of individual uncertainties in the different parts of the pin and also the combined effect of two perturbed radii simultaneously. Uncertainty in the density of the fuel pellet is presented separately (Section 4.1.3). After the 1D results, an overview of the most important outcome of the 2D calculations is given (Sections 4.1.4-4.1.5), which shows the effect of fuel pellet movement inside the pin and the displacement of the pins as a whole in the fuel assembly.

4.1.1 One parameter perturbed

In order to quantify the effect each individual part of the fuel pin has, the radii were perturbed separately one by one. In Table 4.1 below the σ's in the k_{eff} due to the individual perturbations are given. A number of things can be concluded from this. Only the fuel pellet radius has a (strong) positive correlation on the k_{eff}. A bigger radius means more fuel and thus a higher rate of neutron production. All other perturbations have a negative effect on k_{eff}, because in that case more material means simply more absorption of neutrons and thus a higher rate of neutron loss.

A few remarks must be made. Perturbing the cladding on the outside with the same σ as a perturbation on the inside of the ceramic tube does not give the same results. This has two reasons. First, perturbing the outside radius with a certain radius ΔR adds or

Table 4.1: Output results for individual single perturbations. For the fuel pellet, results for $\sigma = 10$ μm is shown, because this value was used later in the research.

Region	σ in input [%]	σ in k_{eff}[%]	Slope regression analysis
Fuel pellet	0.30	0.17642	0.59900
W14Re- liner	2.5	0.05889	-0.02390
Re- liner	10	0.15098	-0.01525
Cladding (inside)	0.97	0.03865	-0.04127
Cladding (outside)	0.97	0.06738	-0.06505

subtracts more material than the same perturbation ΔR on the inside. Second, when a perturbation is made on the inside, this pushes the liners closer or further away from the fuel pellet, which thus also changes their volumes. The same goes for a perturbation of the rhenium liner, which also pushes the tungsten-rhenium liner closer or further away from the fuel pellet. Hence these perturbations actually have a combined effect.

When a positive perturbation is made to the inside of the ceramic tube, resulting in more cladding and thus also in a smaller amount of both liners, there is still a negative effect. The smaller absorption from the liners due to their smaller amount is compensated by the higher absorption in the cladding.

The big effect of the uncertainty due to the fuel pellet deserves some more investigation. To this end, a whole range of values for σ was researched. Each σ value results in a σ value in the k_{eff}. An overview of these results can be found in Figure 4.1. When it is necessary to keep the uncertainty in the k_{eff} below a certain level, the level of uncertainty in the fuel mass (and hence the fuel radius, supposing constant fuel density) should not exceed a certain level. Such a graph can then be used to obtain limits on the needed manufacturing precision for the pellets.

For the rest of this research the uncertainty in the fuel was taken as 10 μm, the same distribution as for the perturbations of the cladding width.

4.1.2 Two parameters perturbed

In order to qualitatively investigate a possible combined effect, two different parts of the fuel pin were perturbed at the same time. All possible combinations were made. An example of a scatter plot from such a calculation is given in Figure 4.2, this is the case of the two metallic liners. One of the perturbations is depicted on the x-axis and the other perturbation is expressed as a color gradient.

There is a clear difference between the two figures. We still see the negative correlation on k_{eff} for both, but when the perturbation of the tungsten-rhenium liner is plotted against k_{eff} with the perturbation of the rhenium liner as color gradient, the graph shows a much more spread picture than when we plot the perturbation of the rhenium

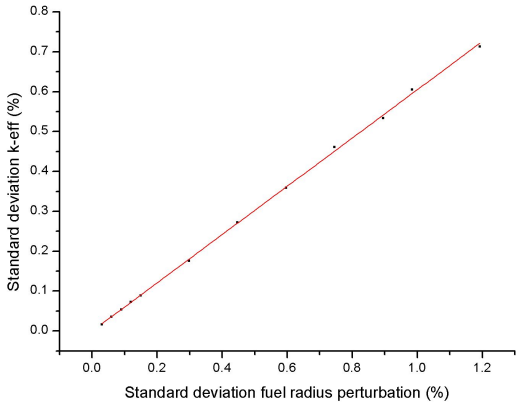

Figure 4.1: Range of σ values for the uncertainty in the fuel pellet. The linear interpolation is y = -0.00029 + 0.60561 x

liner with the tungsten-rhenium liner as color gradient. This spread is reflected in $\hat{R}^2$ as well, which gives 0.10124 for the first graph (Figure 4.2a) and 0.86743 for the second graph (Figure 4.2b). This clearly shows that the dominant effect is the width of the pure rhenium liner in this case.

In Table 4.2 an overview is given for the different values of $\hat{R}^2$ for the different double perturbations. As expected from the first results, the fuel has a dominating effect. The most striking result is the influence of the rhenium liner, which dominates in almost every combination made. Again we see that perturbations made on the outside of the cladding have a bigger effect than on the inside, which means that the presence of more ceramic material has a bigger effect than the movement of the liners due to a perturbation of the cladding on the inside. Graphs of all combinations can be found in Appendix A.

Table 4.2: Overview of the effect of combinations of perturbations

	Fuel	W14Re-liner	Re-liner	Cladding (inner)	Cladding (outer)
Fuel	-	0.89769	0.55912	0.94595	0.88874
W14Re-liner	0.09914	-	0.10124	0.70792	0.46842
Re-liner	0.43706	0.86743	-	0.93297	0.85542
Cladding (inner)	0.05328	0.28187	0.06945	-	0.31782
Cladding (outer)	0.12744	0.54179	0.14149	0.71276	-

For every perturbation combination the uncertainty or σ in the k_{eff} was determined. It is expected that when more uncertainty is added to the input of the system, more uncertainty, or a bigger σ emerges in the output, and the results clearly underline this. In Figure 4.3 an overview is given of the various values of σ in the k_{eff}. As mentioned before, the uncertainty for the fuel was taken as 10 μm.

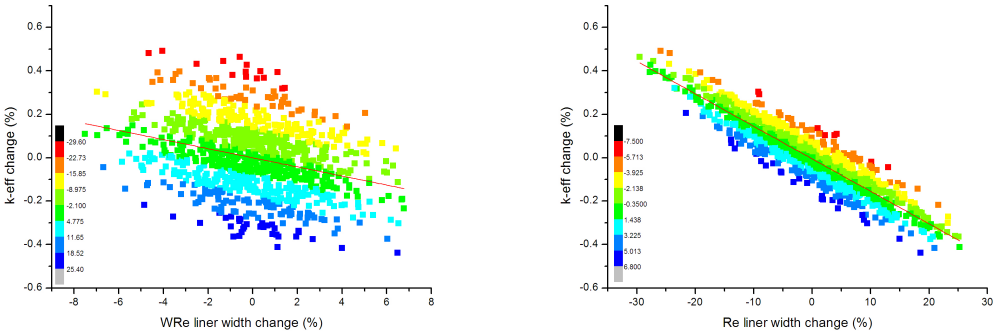

(a) W14Re - liner

(b) Re - liner

Figure 4.2: Scatter plots of the combined effect of the W14Re - liner and the Re - liner

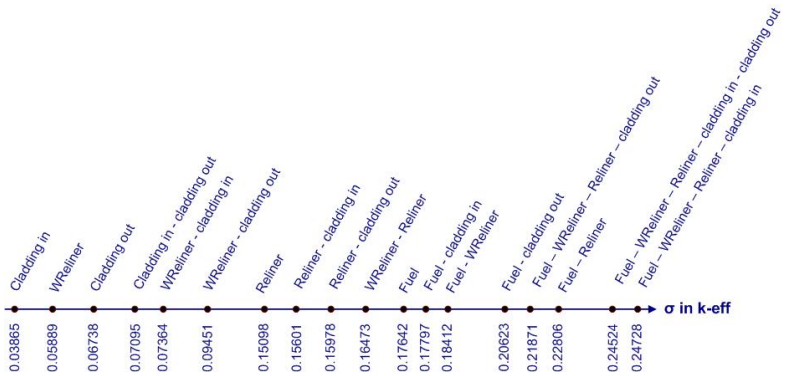

Figure 4.3: Overview of σ in the output parameter k_{eff}

As expected from the results above, any combination involving the fuel or the rhenium liner result in a higher uncertainty in the output. When all possible radii are perturbed, the final uncertainty in the k_{eff} is $\sigma = 0.25\%$.

4.1.3 Fuel density modification

Uncertainty in the fuel radius can result from uncertainty in the fuel mass, with the density assumed precise or from uncertainty in the density of the fuel with the mass assumed precise. So far, the first was assumed. In this section, an overview of the results from the research on the uncertainty in the k_{eff} due to the uncertainty in the density is presented.

The difference between the two are significant. Where the uncertainty in the mass leads to a very strong effect on the k_{eff}, for every 1% change in the radius there is a change in

Table 4.3: Comparison between density and mass perturbation

Comparison between fuel radius perturbation without and with density modification

	σ in k_{eff}	Slope regression analysis
With mass modification	0.17642	0.59900
With density modification	5.13939E-4	-0.00181

the k_{eff} of almost 0.6%, the uncertainty in the density leads to a very small (300 times smaller) and even negative effect.

When not only the fuel radius was perturbed, but also one of the other radii, this effect was confirmed. The regression slope has the same value as if only that specific radius was changed. As an example, in Figure 4.4 it is easy to see the (lack of) effect from uncertainty in the density.

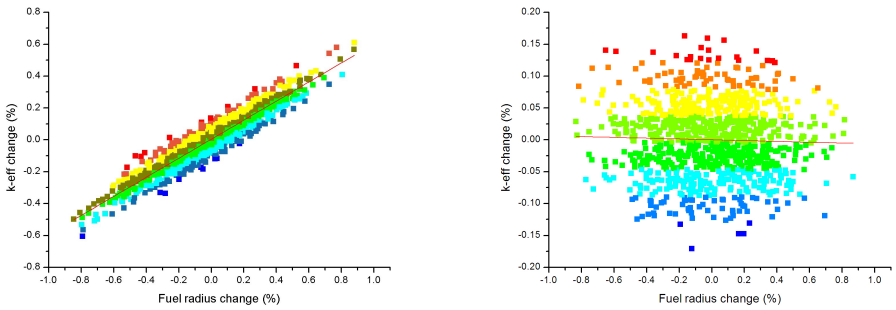

(a) With mass uncertainty

(b) With density uncertainty

Figure 4.4: Scatter plots of the combined effect of the fuel and the WRe liner perturbed, the left is with mass uncertainty and the right with density uncertainty

In the rest of this report it is always assumed that the uncertainty in the fuel pin arises from uncertainty in the mass, with the density being constant.

4.1.4 Fuel pellet displacement inside the pin

When the fuel pellets can move freely within the cladding, the effect on the k_{eff} is smaller than 0.1 pcm, and thus smaller than the scope of NEWT. Reason for this lack of effect is that the maximum perturbation of the position is still a very small distance and that it is not so much the position that dictates changes in the k_{eff}, but rather the ratio between the different materials.

4.1.5 Pin displacement

Multiple σ's in the Gaussian distribution of the pin position have been tried to see an effect of the pin displacement. Measurements with $\sigma = 1$ μm and $\sigma = 10$ μm were aborted prematurely when no changes were seen in the k_{eff}. Increasing the σ to 100 μm gave a maximum change of 10^{-6} in the k_{eff}, the last digit SCALE is able to calculate. This is a very similar effect to the pellet displacement

The explanation for this lack of result can be found in the fact that it is a fast reactor. Cross sections are smaller than in thermal reactors, resulting in a larger mean free path for neutrons, which means that it is not so much the positions of the pins that matters, but rather the volume fractions of the different materials in the core.

Because there was so little effect for these perturbations, the extreme value of $\sigma = 400$ μm was tried. For larger values of σ, the overlapping of pins would become a serious issue, because the distance between two pins is 2.41 mm. With this value of σ already a number of measurements were stopped by NEWT because of overlapping pins. Because of time-management issues, it was not possible to run a full data set of 1000 data points, but only 250.

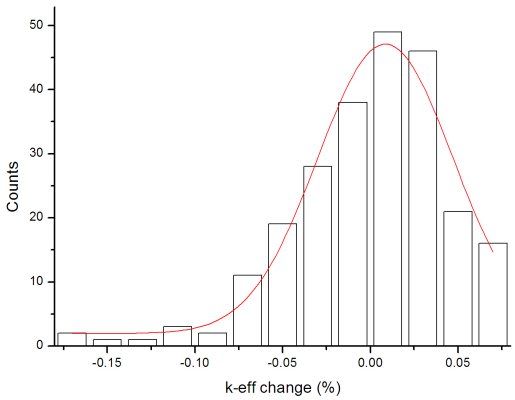

Figure 4.5: Distribution of the k_{eff} when fuel pin positions are perturbed with a Gaussian distribution with $\sigma = 400$ μm

The σ in the k_{eff} is just 0.03858, which is comparable to the uncertainty in the output resulting from one single radius perturbed. The graph shows only a left wing and no right wing. Unfortunately a satisfactory explanation for this phenomenon was not found.

4.2 Thermal-hydraulics

For the thermal-hydraulics section the results are divided in two parts. The first subsection gives an overview of the most important outcome regarding the effect of perturbed radii on the average and maximum temperature in different parts of the fuel pin. The second subsection gives an overview of the results in the power densities.

4.2.1 Temperature profile

Temperature, and especially the maximum temperature in the different materials, is a critical factor to be considered in reactor design. Too high maximum temperatures can cause a too low safety margin between the operating temperature and temperatures where material integrity can no longer be guaranteed.

The total heat produced per fuel pin was modeled as constant. The coolant temperature along the pin is only dependent on the given inlet temperature of the reactor and the pin power, hence was not changed by the perturbations. The temperature profile in the fuel pellet is parabolically shaped, with a maximum at the center of the fuel pellet. The average temperature is around 1400 K and the maximum temperature around 1600 K. The helium in the gap is not a good heat conductor and this gap causes a temperature drop of on average 125 K. The liners both are very good conductors, so the temperature drop is small and they both have an average temperature of around 1200 K. The SiC cladding is again not a very good heat conductor, there is a temperature drop of on average 50 K. With a modelled maximum temperature (in the fuel) and a known outside coolant temperature, the total temperature drop over the fuel pin is known. In Figure 4.6 an average radial temperature profile is presented.

The effect of geometrical uncertainties in the fuel pin were investigated by looking at the average and maximum temperatures in the different parts of the fuel pin. These data were then converted to percentual values, so the relative effect of the perturbations can be seen.

Correlation between one perturbed parameter and the average temperatures

It can be seen from Table 4.4 that perturbation of the cladding width has the largest effect. A thicker cladding means that there is more heat resistance, causing an overall increase of the average temperatures in the other regions. A 1% increase in cladding thickness, increases the average temperatures in the different regions by $0.035 - 0.085\%$.

Perturbation of the fuel pellet radius also has quite an effect on the average temperature. A larger fuel pellet radius decreases the gap between the fuel pellet and the liners, which causes a smaller temperature drop over the gap. This means that in every region

Figure 4.6: Radial temperature profile of a GFR2400 fuel pin

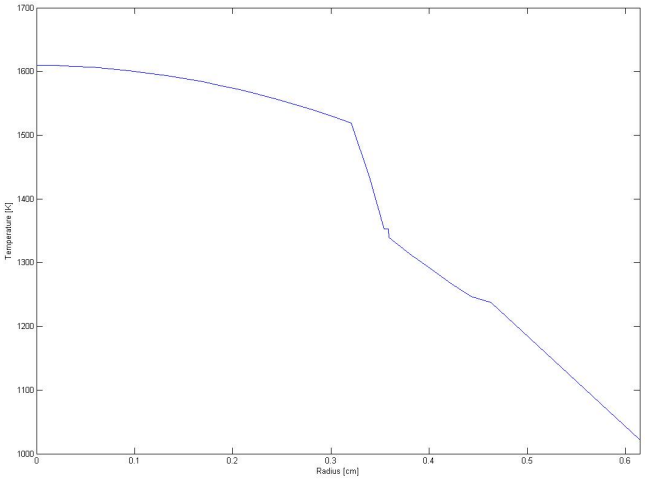

Table 4.4: Effect of geometrical uncertainties on the average temperature in different parts of the fuel pin. Effects are expressed as the slope of the regression analysis performed on the data

Region perturbed	T_{fuel}	T_{Hegap}	$T_{W14Reliner}$	$T_{Reliner}$	$T_{cladding}$
Fuel pellet	-0.10723	-0.06355	-0.01057	-0.01056	-0.01033
W14Re liner	$1.23 \cdot 10^{-4}$	$1.81 \cdot 10^{-4}$	$9.28 \cdot 10^{-5}$	$-4.98 \cdot 10^{-5}$	$-4.30 \cdot 10^{-5}$
Re liner	$-2.43 \cdot 10^{-5}$	$-2.07 \cdot 10^{-6}$	$9.55 \cdot 10^{-6}$	$-3.75 \cdot 10^{-5}$	$-8.73 \cdot 10^{-5}$
Cladding	0.0645	0.0752	0.0844	0.0844	0.0363

the average temperature decreases due to the increased gap conductance. The fuel pellet radius perturbation has the largest impact on the average fuel temperature, which decreases 0.1% for a 1% radius increase.

The effect of the liners on the average temperatures is very small and could even be the result of imprecisions in either XSDRN or the thermal-hydraulics code.

Correlation between one perturbed parameter and the maximum temperatures

Again the uncertainty in the fuel pellet and the cladding have the biggest effect, for example an increase of 1% in the cladding width increases the maximum temperature in every part of the fuel pin by 0.08%.

The thicker cladding decreases the heat conduction and increases the maximum temperature everywhere. When the cladding is perturbed on the inner side of the tube,

Table 4.5: Effect of geometrical uncertainties on the maximum temperature in different parts of the fuel pin. Effects are expressed as the slope of the regression analysis performed on the data.

Region perturbed	T_{fuel}	T_{Hegap}	$T_{W14Reliner}$	$T_{Reliner}$	$T_{cladding}$
Fuel pellet	-0.0509	-0.02665	0.00976	0.00969	0.00660
W14Re liner	$1.77 \cdot 10^{-3}$	$1.27 \cdot 10^{-3}$	$8.57 \cdot 10^{-4}$	$7.27 \cdot 10^{-4}$	$6.12 \cdot 10^{-4}$
Re liner	$7.49 \cdot 10^{-4}$	$5.19 \cdot 10^{-4}$	$3.85 \cdot 10^{-4}$	$3.41 \cdot 10^{-4}$	$2.50 \cdot 10^{-4}$
Cladding	0.0822	0.0866	0.0875	0.0874	0.0752

this also goes at the expense of the helium gap, which would decrease the maximum temperature of the fuel. However, the effect of the thicker cladding compensates more than enough for this. An increased fuel radius goes at the expense of the helium gap. This increases the heat conduction and thus gives a lower maximum temperature in the fuel, but higher ones in the cladding and the liners.

Again the liners have a minimal effect on the temperature profile, mostly because of their high conductivity.

Uncertainty in thermal-hydraulic results

Not only the correlation between a perturbed radius and the average and maximum temperature is important, but also the uncertainty in these results. Because only a perturbed fuel pellet radius and cladding width appear to have an effect on the temperature profile, only the uncertainty is these quantities is given here, for the uncertainty in the liners, the reader is referred to Appendix B.

Table 4.6: Overview of the uncertainties in thermal-hydraulic parameters due to fuel pellet and cladding perturbations

Parameter	Fuel perturbed		Cladding perturbed	
	σ [%] average	σ [%] maximum	σ [%] average	σ [%] maximum
T_{fuel}	0.02809	0.01109	0.06497	0.08583
T_{Hegap}	0.01597	0.00401	0.07682	0.08986
$T_{W14Reliner}$	0.00446	0.00752	0.08789	0.09151
$T_{Reliner}$	0.00446	0.00751	0.08789	0.09175
$T_{cladding}$	0.00424	0.00655	0.03649	0.07571

As can be seen from Table 4.6 the uncertainty in the cladding width introduces a much larger uncertainty in the thermal parameters, not just in one value, but in every temperature region measured.

4.2.2 Power density profile

In order to investigate the effect geometrical uncertainties have on the power of a fuel pin, the power density profile was studied. Each radius was perturbed independently to see the individual effects. For each perturbation series the flux was converted to a power density profile, from which the maximum power density value, the average power density value and the power peaking factor (which is the ratio of the maximum and the average power density) can be extracted. These data were then converted to percentual values, so the relative effect of the perturbations can be seen.

Correlation between one perturbed parameter and the power densities

The power for one individual fuel pin was always set to the same value, so when the radius of the fuel pellet is increased and thus the power producing volume of the fuel pin as well, the average power density decreases. For the perturbations of the other radii, the average power density of the pin is not affected. This is expected as the volume of the fuel is always the same.

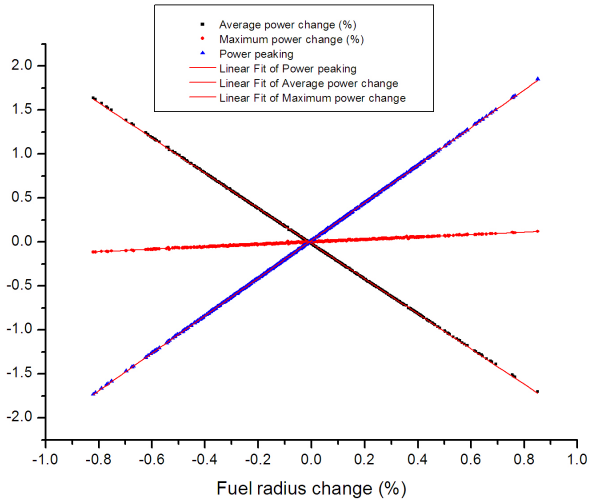

Figure 4.7: Effect of the geometrical uncertainty in the fuel pin on average and maximum power density as well as the power peaking factor

The maximum power density in the fuel pin is less dependent on the radius perturbation, as is clearly shown in Figure 4.7 for the perturbation of the fuel pin. For the fuel pellet perturbation the effect on the maximum power density is almost 15 times smaller than the effect on the average power density. Perturbations in any other radius gives an even smaller effect than for the fuel pellet perturbation. In Table 4.7 an overview of these results is given.

Table 4.7: Overview of the effects of the various perturbations on the average and maximum power density, effects are expressed as the slope of the regression analysis performed on the data

Region	Average power density	Maximum power density	Power peaking factor
Fuel pellet	-2.0042	0.13818	2.13851
W14Re liner	–	0.00492	0.00492
Re liner	–	0.00216	0.00216
Cladding	–	0.03655	0.03655

As can be seen from Table 4.7 the effect of geometrical uncertainties in the fuel pin, with the exception of the fuel pellet radius, have very little effect on the power density profile and thus on the power peaking factor.

Uncertainty in power density parameters

As expected from the effect of individual perturbations on the power density, the only parameter that really has an influence on the uncertainty is the perturbation of the fuel pellet radius, which introduces a σ of 0.55% in the average power density and a σ of 0.58% in the power peaking. An overview of the other uncertainties in the power density parameters are given in Table 4.8.

Table 4.8: Overview of the uncertainties in the power density parameters

Region perturbed	σ in $P_{avg}[\%]$	σ in $P_{max}[\%]$	σ in power peaking
Fuel pellet radius	0.55381	0.03756	0.58745
WReliner width	-	0.01213	0.01227
Reliner width	-	0.02531	0.02534
Cladding width	-	0.03780	0.03792

Chapter 5

Conclusions and recommendations

This research investigated some of the geometrical uncertainties in the GFR2400 design. In this chapter the most important results are repeated. The chapter ends with some recommendations for future work.

5.1 Conclusions

Uncertainty in the fuel The uncertainty in the fuel pellet radius has a bigger effect on the uncertainty in the k_{eff} than any other uncertainty in the fuel pin geometry. The uncertainty in the fuel pellet radius introduces a uncertainty with a σ of 0.17% in the k_{eff}. This effect is solely due to an uncertainty in the mass of the fuel. The effect on the uncertainty in k_{eff} nearly vanishes when the mass is kept constant and the density is properly modified.

Uncertainty in the liners The uncertainty in the liners has a relatively large negative impact on the k_{eff}. The rhenium liner shows the biggest effect, because of its higher absorption cross section. The uncertainty in the rhenium liner introduces a uncertainty with a σ of 0.15% in the k_{eff}, comparable to the uncertainty introduced by a uncertain fuel pellet radius.

Uncertainty in the ceramic cladding The uncertainty in the outer radius has a bigger effect on the k_{eff} than the uncertainty in the inner radius of the ceramic tube. Uncertainty at the inner radius of the tube compensates for the lower or higher absorption of the liners, as they are moved closer or further away according to the perturbation at the inner radius.

Uncertainty in the pin position Fuel pellet movement within the cladding has no effect on the k_{eff}. Displacement of the whole fuel pin only results in a very small effect, which can only be calculated at relatively large perturbations.

Temperature profile Uncertainty in the fuel pellet radius and cladding width are the main contributors to an uncertainty in the average and maximum temperature in different parts of the fuel pin. An increase of 1% in the radius of the pin leads to a decrease of 0.01-0.1% in the average temperatures, while that of the width of the cladding gives an increase in maximum temperatures between 0.035% and 0.085%. The maximum uncertainty introduced in the output parameters is caused by a cladding width perturbation and has a maximum σ of 0.09%.

Power densities The only geometrical uncertainty with any significant influence on the power density, is the uncertainty in the fuel pellet radius. The power peaking factor increases with 2% when the fuel pellet radius increases 1%. The maximum uncertainty caused by this perturbation is a σ of 0.58%.

5.2 Recommendations for further research

Experimental The choice of σ in most cases was a based on intuition. Material tests should be performed to see if our choices of σ were justified.

This research could serve as the start of a guideline for the production tolerance allowed in the manufacturing process for the several components of the fuel pin.

Computational In this research there was only time to investigate the influence of a single perturbed radius on the power density of a single fuel pin. This could be expanded to the influence of any combination of parameters on the power density.

The 1D model could be further expanded to take into account the uncertainty in the ratio of uranium and plutonium isotopes in the fuel.

The 2D model could be expanded by including the two different fuel regions.

Bibliography

[1] L.L. Briggs. Uncertainty quantification approaches for advanced reactor analyses. Technical report, Argonne National Laboratory, September 2008.

[2] Forrest B. Brown. Fundamentals of Monte Carlo particle transport. In *Lecture notes for Monte Carlo course*. Los Alamos National Laboratory, 2005.

[3] Dan G. Cacuci and Mihaela Ionescu-Bujor. A comparative review of sensitivity and uncertainty analysis of large-scale systems - II: Statistical methods. *Nuclear Science and Engineering*, 147:204–217, July 2004.

[4] M.D. DeHart. *NEWT: a new transport algorithm for two-dimensional discrete ordinates analysis in non-orthogonal geometries*. Nuclear Science and Technology Division, January 2009.

[5] Prof. John Deutch and prof. Ernest J. Moniz e.a. The future of nuclear power. Technical report, Massachusetts Institute of Technology, 2003.

[6] James J. Duderstadt and Louis J. Hamilton. *Nuclear reactor analysis*. John Wiley and Sons, Inc., 1976.

[7] Dekking e.a. *A modern introduction to probability and statistics*. Springer - Verlag London Limited, 2005.

[8] Euratom FP7 GoFastR Collaborative Project, GIF GFR System Steering Committee. *The Gas-Cooled Fast Reactor and Generation IV*.

[9] N.M. Greene and L.M. Petrie. *XSDRNPM: a one-dimensional discrete-ordinates code for transport analysis*. Nuclear Science and Technology Division, January 2009.

[10] Oak Ridge National Laboratory. SCALE.

[11] OriginLab Coorporation, Northampton, USA. *Origin 8 Reference v8*.

[12] Zoltàn Perkó. GFR2400 core neutronics characterisation. Technical report, TU Delft, 2011.

[13] U.S. DOE Nuclear energy research advisory committee and the generation IV international forum. *A technology roadmap for generation IV Nuclear Energy Systems*, December 2002.

[14] Maxime Zabiégo. Nuclear fuel design and associated material issues. In *GoFastR Course*. CEA/DEN/CAD/DEC/SESC/LC2I, June 2011.

Appendix A

Neutronics results

In this Appendix an elaborate overview of the neutronics results is given. Figures A.1-A.16 show the effect of one perturbed parameter on the output parameter k_{eff}. Both the linear regression slope and the distribution of k_{eff} are given. Figures A.17-A.26 show the results for two parameters perturbed. Color gradients are similar to those in Figure 4.2. Again the linear regression slope and distribution of k_{eff} are given. Figure A.27 shows the distributions for the k_{eff} when more than two parameters are perturbed.

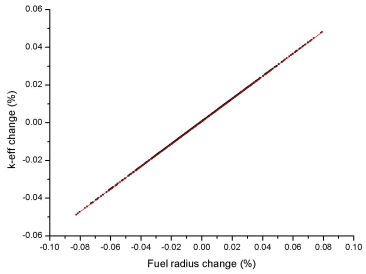

(a) Fuel radius vs k_{eff}
slope = 0.59848

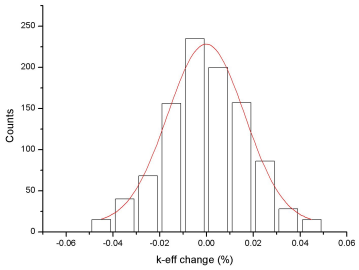

(b) Distribution of k_{eff}
$\sigma = 0.01648\%$

Figure A.1: Correlation between perturbed fuel radius with $\sigma = 1$ μm and k_{eff}

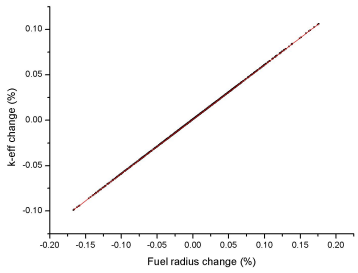

(a) Fuel radius vs k_{eff}
slope = 0.59873

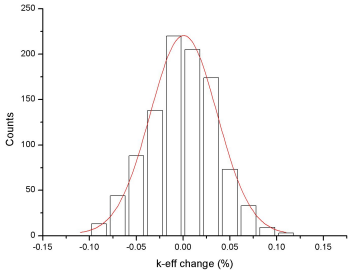

(b) Distribution of k_{eff}
$\sigma = 0.3573\%$

Figure A.2: Correlation between perturbed fuel radius with $\sigma = 2$ μm and k_{eff}

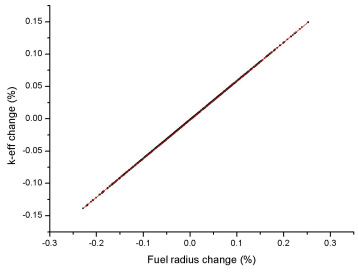

(a) Fuel radius vs k_{eff}
slope = 0.59864

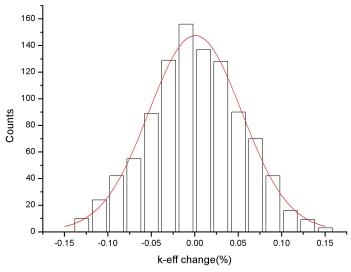

(b) Distribution of k_{eff}
$\sigma = 0.05353\%$

Figure A.3: Correlation between perturbed fuel radius with $\sigma = 3$ μm and k_{eff}

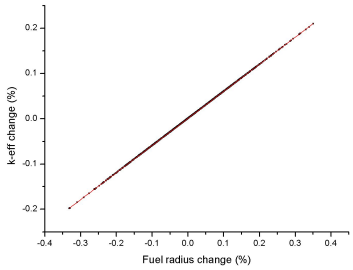

(a) Fuel radius vs k_{eff}
slope = 0.59866

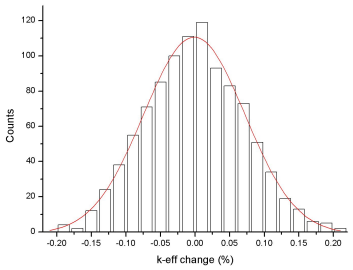

(b) Distribution of k_{eff}
$\sigma = 0.07331\%$

Figure A.4: Correlation between perturbed fuel radius with $\sigma = 4$ μm and k_{eff}

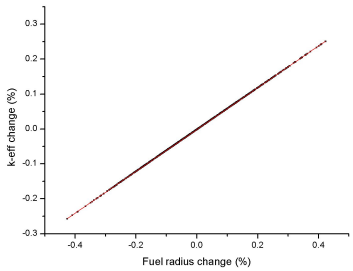

(a) Fuel radius vs k_{eff}
slope = 0.59859

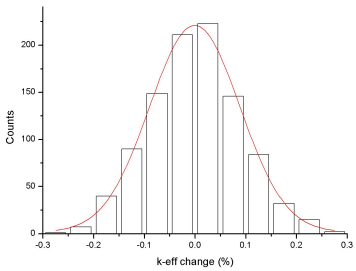

(b) Distribution of k_{eff}
$\sigma = 0.08903\%$

Figure A.5: Correlation between perturbed fuel radius with $\sigma = 5$ μm and k_{eff}

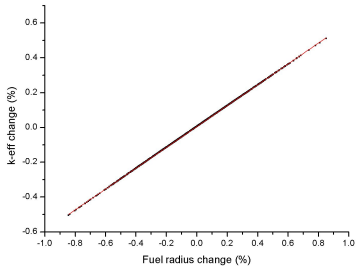

(a) Fuel radius vs k_{eff}
slope = 0.59900

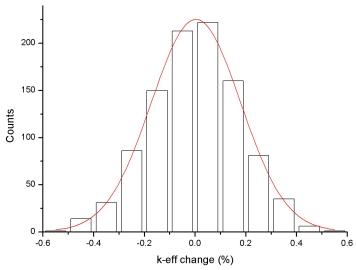

(b) Distribution of k_{eff}
$\sigma = 0.17642\%$

Figure A.6: Correlation between perturbed fuel radius with $\sigma = 10$ μm and k_{eff}

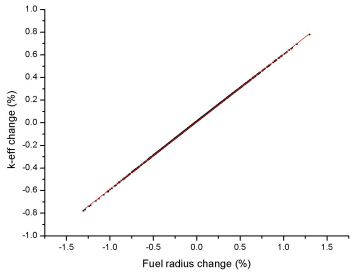

(a) Fuel radius vs k_{eff}
slope = 0.59902

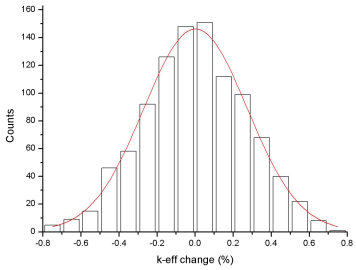

(b) Distribution of k_{eff}
$\sigma = 0.27229\%$

Figure A.7: Correlation between perturbed fuel radius with $\sigma = 15$ μm and k_{eff}

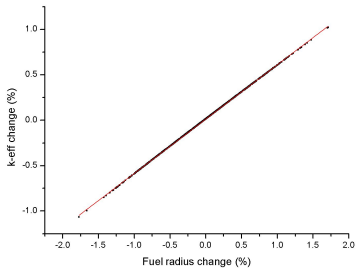

(a) Fuel radius vs k_{eff}
slope = 0.55906

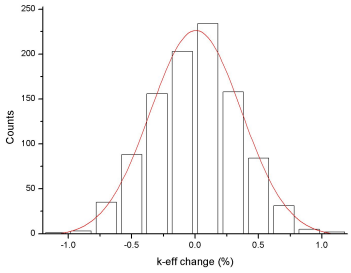

(b) Distribution of k_{eff}
$\sigma = 0.35922\%$

Figure A.8: Correlation between perturbed fuel radius with $\sigma = 20$ μm and k_{eff}

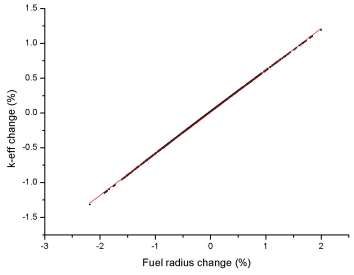

(a) Fuel radius vs k_{eff}
slope = 0.59953

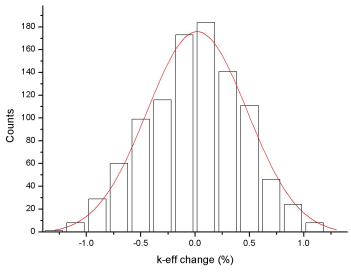

(b) Distribution of k_{eff}
$\sigma = 0.46073\%$

Figure A.9: Correlation between perturbed fuel radius with $\sigma = 25$ μm and k_{eff}

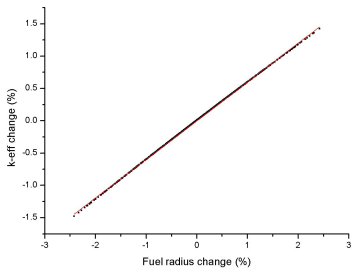

(a) Fuel radius vs k_{eff}
slope = 0.59903

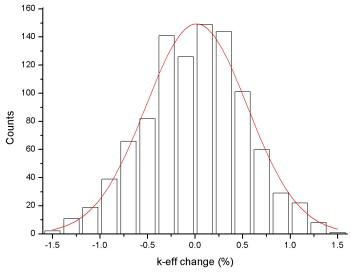

(b) Distribution of k_{eff}
$\sigma = 0.53411\%$

Figure A.10: Correlation between perturbed fuel radius with $\sigma = 30$ μm and k_{eff}

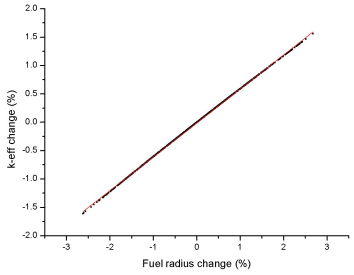

(a) Fuel radius vs k_{eff}
slope = 0.59855

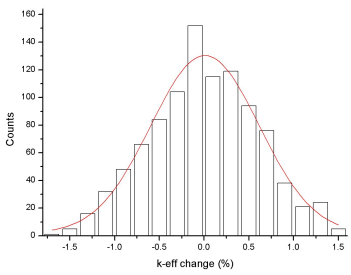

(b) Distribution of k_{eff}
$\sigma = 0.60573\%$

Figure A.11: Correlation between perturbed fuel radius with $\sigma = 33$ μm and k_{eff}

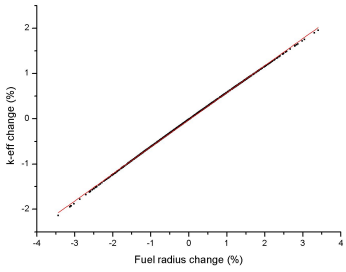

(a) Fuel radius vs k_{eff}
slope = 0.59854

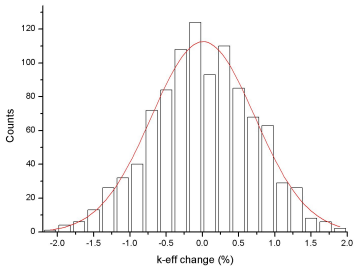

(b) Distribution of k_{eff}
$\sigma = 0.71354\%$

Figure A.12: Correlation between perturbed fuel radius with $\sigma = 40$ μm and k_{eff}

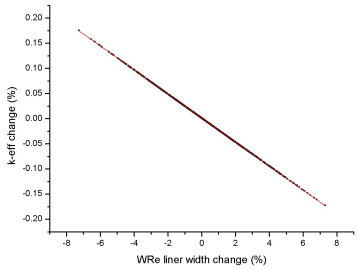

(a) WReliner vs k_{eff}
slope = -0.02390

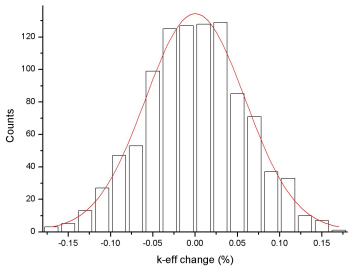

(b) Distribution of k_{eff}
σ = 0.05889%

Figure A.13: Correlation between perturbed WReliner width with $\sigma = 1$ μm and k_{eff}

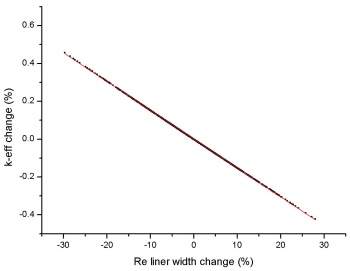

(a) Reliner vs k_{eff}
slope = -0.01525

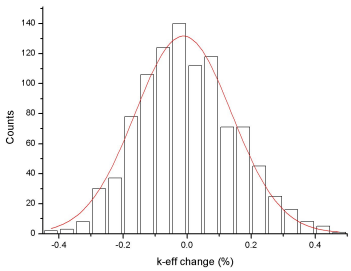

(b) Distribution of k_{eff}
σ = 0.15098%

Figure A.14: Correlation between perturbed Reliner width with $\sigma = 1$ μm and k_{eff}

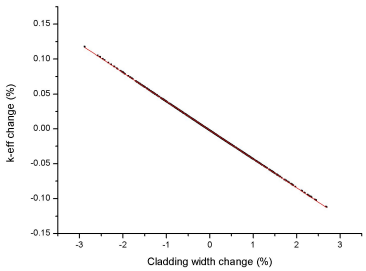

(a) Cladding vs k_{eff}
slope = -0.04127

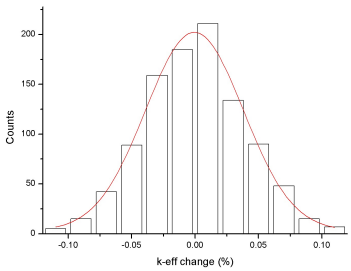

(b) Distribution of k_{eff}
σ = 0.03865%

Figure A.15: Correlation between perturbed cladding width (inside) with $\sigma = 10$ μm and k_{eff}

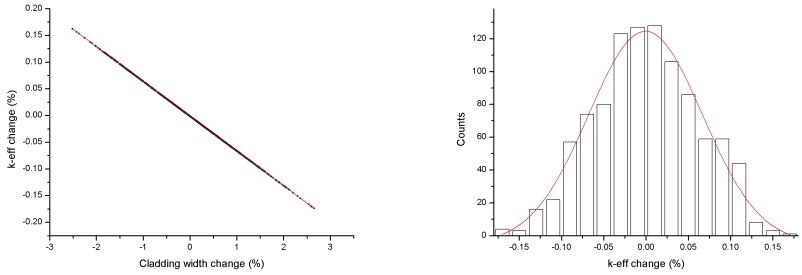

(a) Cladding vs k_{eff}
slope = -0.06505

(b) Distribution of k_{eff}
$\sigma = 0.06738\%$

Figure A.16: Correlation between perturbed cladding width (outside) with $\sigma = 10$ μm and k_{eff}

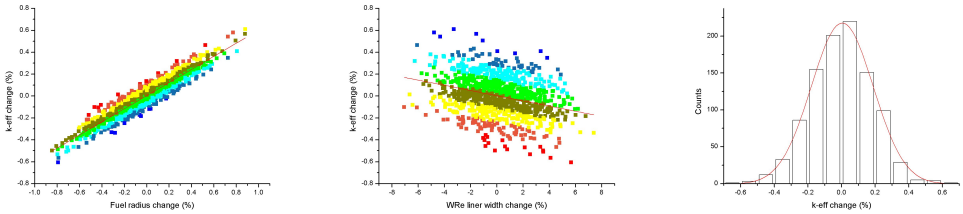

(a) Fuel vs k_{eff} slope = 0.59825

(b) WRe liner vs k_{eff} slope = -0.02364

(c) Distribution of k_{eff} σ = 0.18412%

Figure A.17: Combined effect of perturbed fuel pellet radius and W14Re liner width on k_{eff}

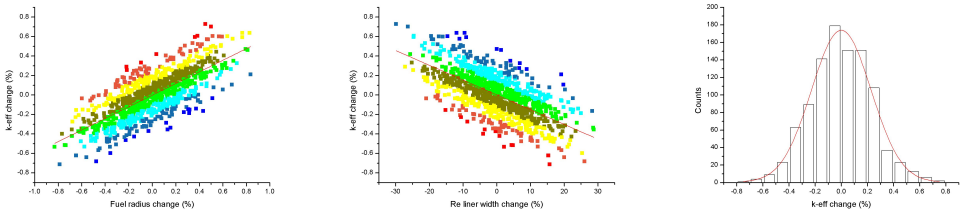

(a) Fuel vs k_{eff} slope = 0.59727

(b) Re liner vs k_{eff} slope = -0.01519

(c) Distribution of k_{eff} σ = 0.22806%

Figure A.18: Combined effect of perturbed fuel pellet radius and W14Re liner width on k_{eff}

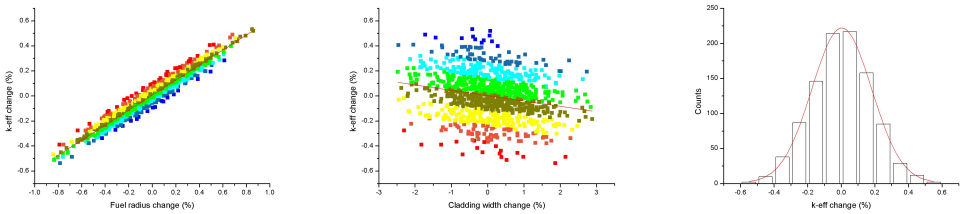

(a) Fuel vs k_{eff} slope = 0.60012

(b) Cladding (inside) vs k_{eff} slope = -0.04270

(c) Distribution of k_{eff} σ = 0.17797%

Figure A.19: Combined effect of perturbed fuel pellet radius and cladding width (inside) on k_{eff}

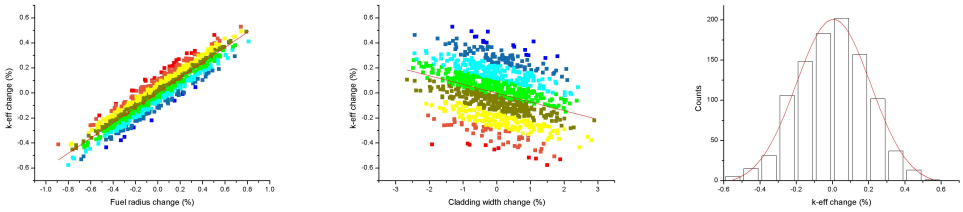

(a) Fuel vs k_{eff}
slope = 0.60445

(b) Cladding (outside) vs k_{eff}
slope = -0.06990

(c) Distribution of k_{eff}
σ = 0.20623%

Figure A.20: Combined effect of perturbed fuel pellet radius and cladding width (outside) on k_{eff}

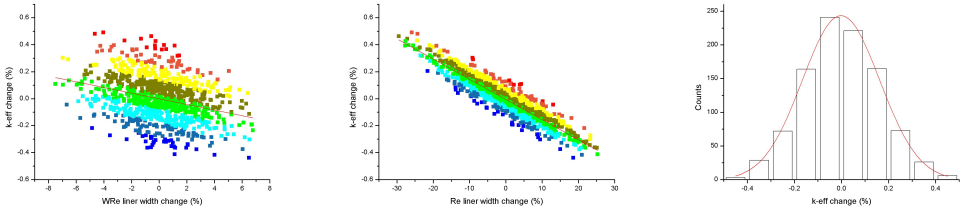

(a) WReliner vs k_{eff}
slope = -0.02098

(b) Reliner vs k_{eff}
slope = -0.01497

(c) Distribution of k_{eff}
σ = 0.16473%

Figure A.21: Combined effect of perturbed WReliner width and Reliner width on k_{eff}

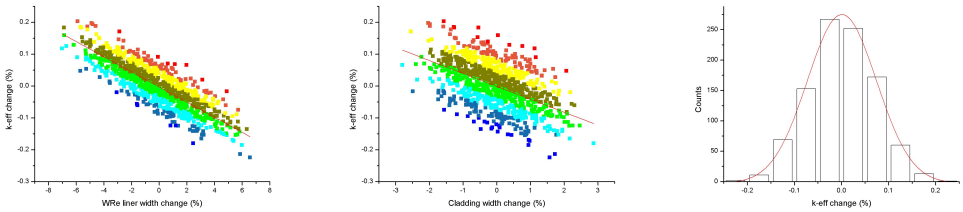

(a) WReliner vs k_{eff}
slope = -0.02374

(b) Cladding (inside) vs k_{eff}
slope = -0.04060

(c) Distribution of k_{eff}
σ = 0.07364%

Figure A.22: Combined effect of perturbed WReliner width and cladding width (inside) on k_{eff}

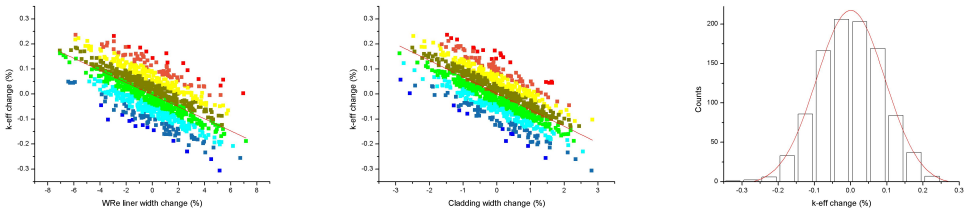

(a) WReliner vs k_{eff}
slope = -0.02419

(b) Cladding (outside) vs k_{eff}
slope = -0.06574

(c) Distribution of k_{eff}
σ = 0.09451%

Figure A.23: Combined effect of perturbed WReliner width and cladding width (outside) on k_{eff}

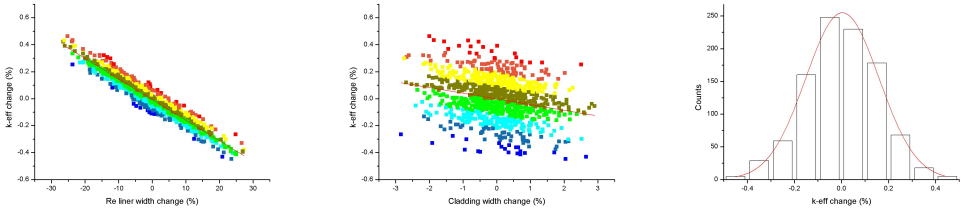

(a) Reliner vs k_{eff}
slope = -0.01526

(b) Cladding (inside) vs k_{eff}
slope = -0.04232

(c) Distribution of k_{eff}
σ = 0.15601%

Figure A.24: Combined effect of perturbed Reliner width and cladding width (inside) on k_{eff}

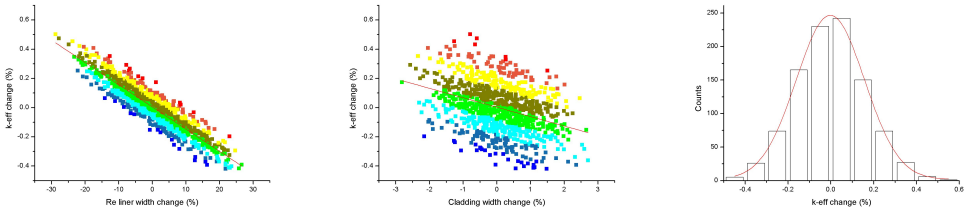

(a) Reliner vs k_{eff}
slope = -0.01522

(b) Cladding (outside) vs k_{eff}
slope = -0.06460

(c) Distribution of k_{eff}
σ = 0.15978%

Figure A.25: Combined effect of perturbed Reliner width and cladding width (outside) on k_{eff}

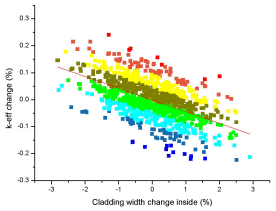

(a) Cladding (inside) vs k_{eff}
slope = -0.04345

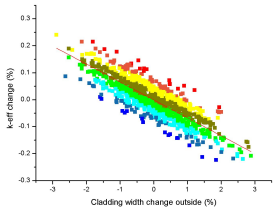

(b) Cladding (outside) vs k_{eff}
slope = -0.06651

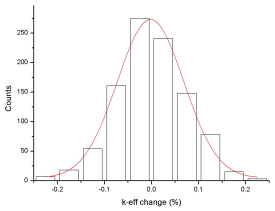

(c) Distribution of k_{eff}
σ = 0.07095%

Figure A.26: Combined effect of perturbed cladding width (inside) and cladding width (outside) on k_{eff}

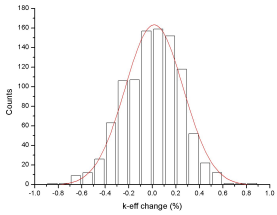

(a) All perturbed
except cladding (outside)
distribution of k_{eff}
σ = 0.24728%

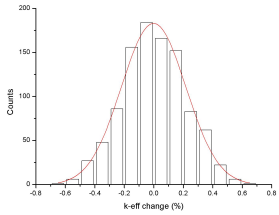

(b) All perturbed
except cladding (inside)
distribution of k_{eff}
σ = 0.21871%1

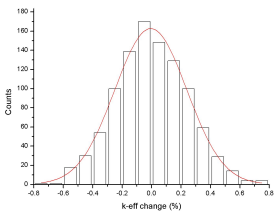

(c) All perturbed
distribution of k_{eff}
σ = 0.24524%

Figure A.27: Combined effect of multiple parameters perturbed on k_{eff}

Appendix B

Thermal-hydraulic results

In this Appendix an elaborate overview of the thermal-hydraulic results is given. First the correlation between the perturbed region and the thermal parameters is given. For each perturbation this means the correlation between the perturbed radius and the maximum or average temperature in a particular region of the fuel pin and how these quantities are distributed.

Second the correlation between the perturbed region and the power density parameters is summarized. For each perturbation this means the correlation between the perturbed radius and the average or maximum power density or the power peaking factor and the distribution of these quantities.

Outlying data points (some of which are still present in the pictures) were found to disappear when the temperature profile for these data points was recalculated. Unfortunately the reason behind these deviations was not found.

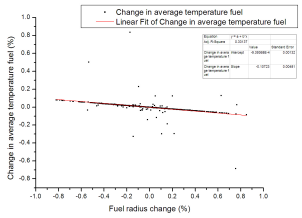

(a) Fuel radius vs $T_{avg,fuel}$
slope = -0.10723

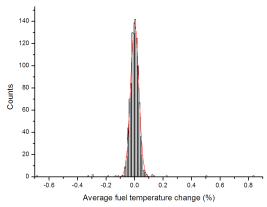

(b) Distribution of $T_{avg,fuel}$
σ = 0.02809%

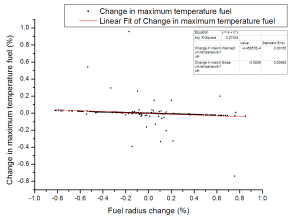

(c) Fuel radius vs $T_{max,fuel}$
slope = -0.0509

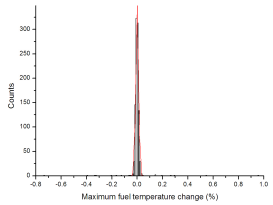

(d) Distribution of $T_{max,fuel}$
σ = 0.01109%

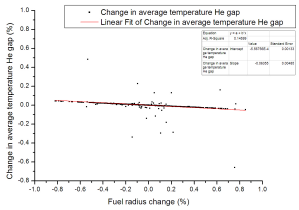

(e) Fuel radius vs $T_{avg,Hegap}$
slope = -0.06355

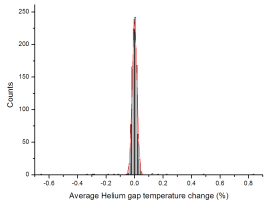

(f) Distribution of $T_{avg,Hegap}$
σ = 0.01597%

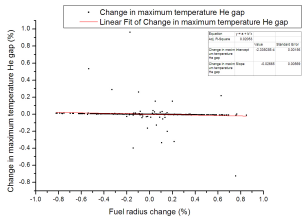

(g) Fuel radius vs $T_{max,Hegap}$
slope = -0.02665

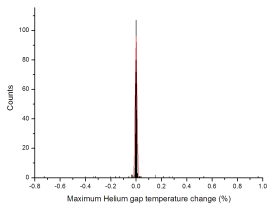

(h) Distribution of $T_{max,Hegapl}$
σ = 0.00401%

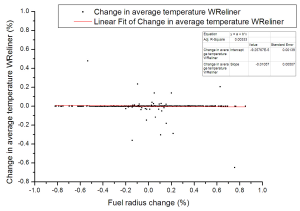

(i) Fuel radius vs $T_{avg,WReliner}$
slope = -0.01057

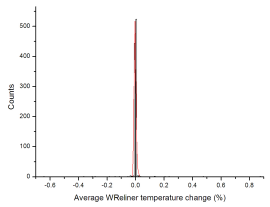

(j) Distribution of $T_{avg,WReliner}$
σ = 0.00446%

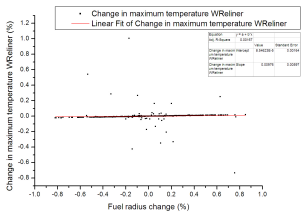

(k) Fuel radius vs $T_{max,WReliner}$
slope = 0.00976

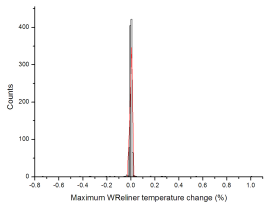

(l) Distribution of $T_{max,WReliner}$
σ = 0.00752%

Figure B.1: Correlation between fuel pellet radius perturbed and thermal parameters

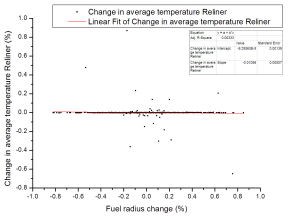

(m) Fuel radius vs $T_{avg,Reliner}$
slope = -0.01056

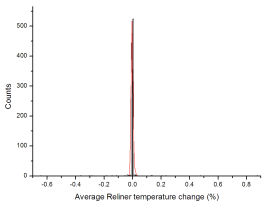

(n) Distribution of $T_{avg,Reliner}$
σ = 0.00446%

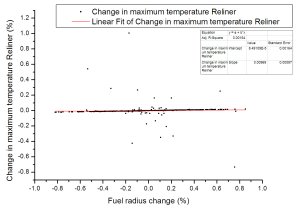

(o) Fuel radius vs $T_{max,Reliner}$
slope = 0.00969

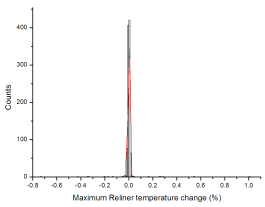

(p) Distribution of $T_{max,Reliner}$
σ = 0.00751%

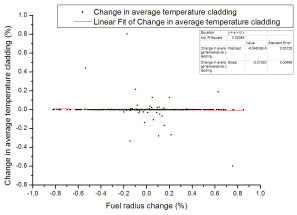

(q) Fuel radius vs $T_{avg,cladding}$
slope = -0.01033

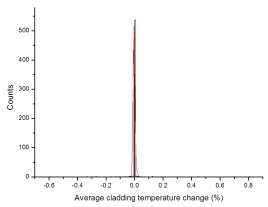

(r) Distribution of $T_{avg,cladding}$
σ = 0.00424%

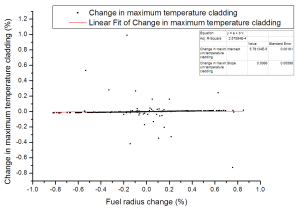

(s) Fuel radius vs $T_{max,cladding}$
slope = 0.0066

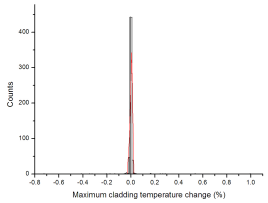

(t) Distribution of $T_{max,cladding}$
σ = 0.00655%

Figure B.1: Correlation between fuel pellet radius perturbed and thermal parameters

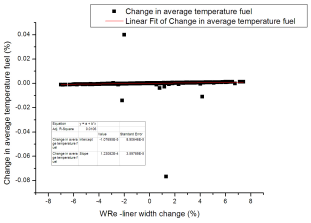

(a) WReliner width vs $T_{avg,fuel}$
slope = 1.23E-4

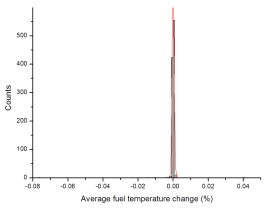

(b) Distribution of $T_{avg,fuel}$
σ = 4.84E-4%

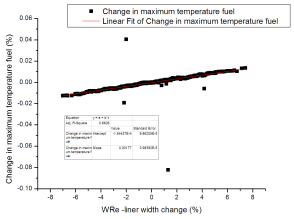

(c) WReliner width vs $T_{max,fuel}$
slope = 1.77E-3

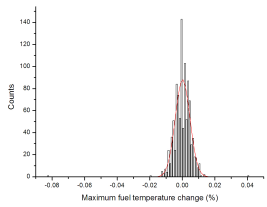

(d) Distribution of $T_{max,fuel}$
σ = 4.51E-3%

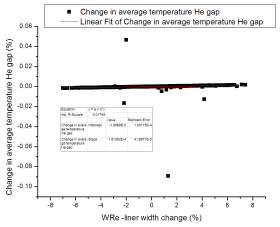

(e) WReliner width vs $T_{avg,Hegap}$
slope = 1.81E-4

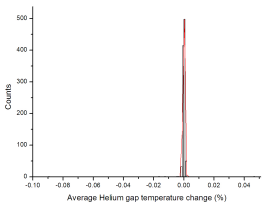

(f) Distribution of $T_{avg,Hegap}$
σ = 6.38E-4%

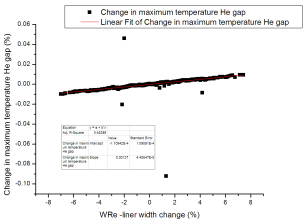

(g) WReliner width vs $T_{max,Hegap}$
slope = 1.27E-3

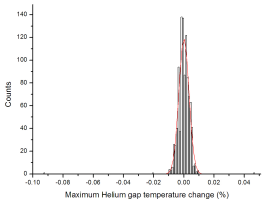

(h) Distribution of $T_{max,Hegapl}$
σ = 3.36E-3%

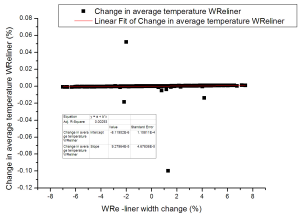

(i) WReliner width vs $T_{avg,WReliner}$
slope = 9.28E-5

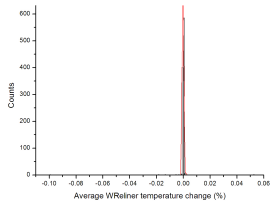

(j) Distribution of $T_{avg,WReliner}$
σ = 4.57E-4%

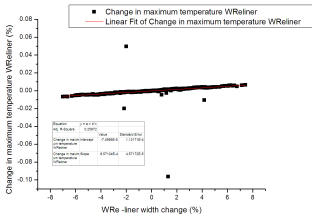

(k) WReliner width vs $T_{max,WReliner}$
slope = 8.57E-4

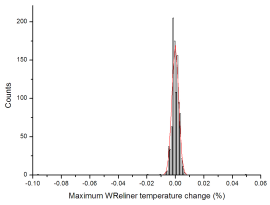

(l) Distribution of $T_{max,WReliner}$
σ = 2.37E-3%

Figure B.2: Correlation between WRe liner width perturbed and thermal parameters

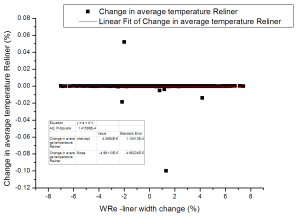

(m) WReliner width vs $T_{avg,Reliner}$
slope = -4.98E-5

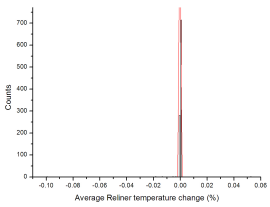

(n) Distribution of $T_{avg,Reliner}$
σ = 2.76E-4%

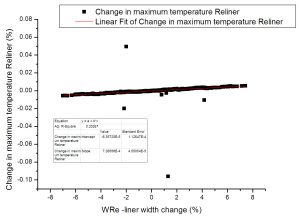

(o) WReliner width vs $T_{max,Reliner}$
slope = 7.27E-4

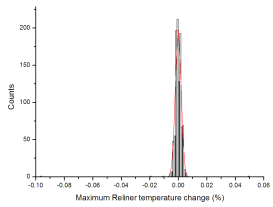

(p) Distribution of $T_{max,Reliner}$
σ = 2.03E-3%

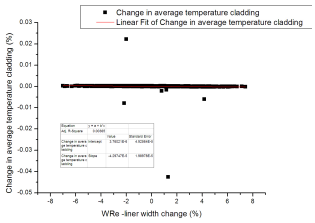

(q) WReliner width vs $T_{avg,cladding}$
slope = -4.30E-5

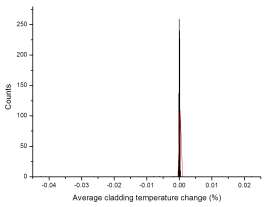

(r) Distribution of $T_{avg,cladding}$
σ = 1.48E-4%

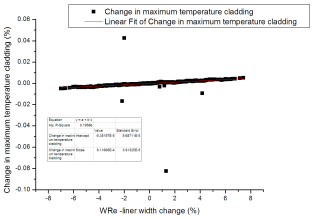

(s) WReliner width vs $T_{max,cladding}$
slope = 6.12E-4

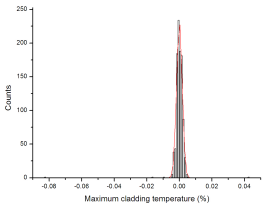

(t) Distribution of $T_{max,cladding}$
σ = 1.74E-3%

Figure B.2: Correlation between WRe liner width perturbed and thermal parameters

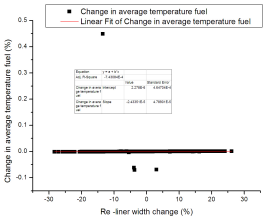

(a) Reliner width vs $T_{avg,fuel}$
slope = 1-2.43E-5

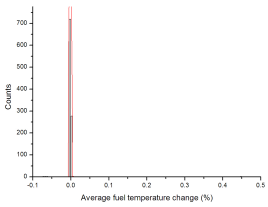

(b) Distribution of $T_{avg,fuel}$
σ = 1.38E-3%

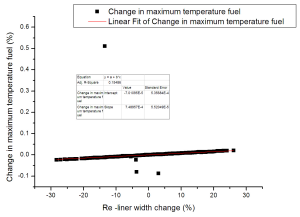

(c) Reliner width vs $T_{max,fuel}$
slope = 8.79E-3

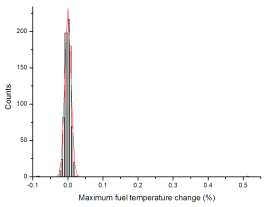

(d) Distribution of $T_{max,fuel}$
σ = 7.49E-4%

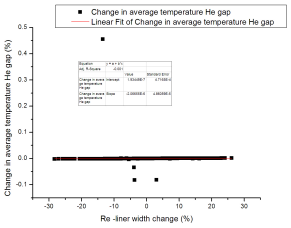

(e) Reliner width vs $T_{avg,Hegap}$
slope = -2.07E-6

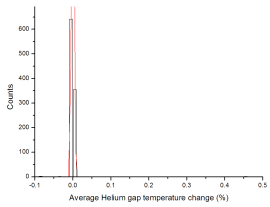

(f) Distribution of $T_{avg,Hegap}$
σ = 2.75E-3%

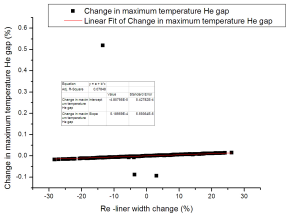

(g) Reliner width vs $T_{max,Hegap}$
slope = 5.19E-4

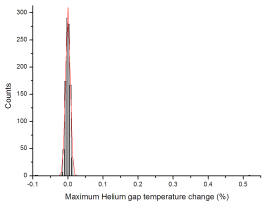

(h) Distribution of $T_{max,Hegapl}$
σ = 6.53E-3%

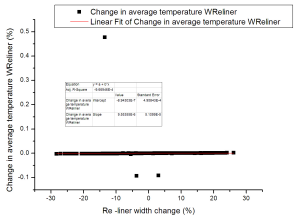

(i) Reliner width vs $T_{avg,WReliner}$
slope = 9.55E-6

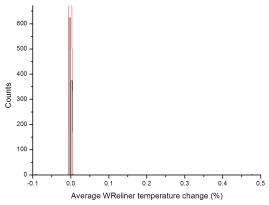

(j) Distribution of $T_{avg,WReliner}$
σ = 1.32E-3%

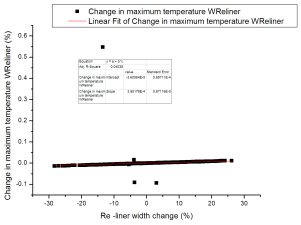

(k) Reliner width vs $T_{max,WReliner}$
slope = 3.85E-4

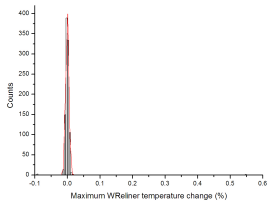

(l) Distribution of $T_{max,WReliner}$
σ = 4.80E-3%

Figure B.3: Correlation between Re liner width perturbed and thermal parameters

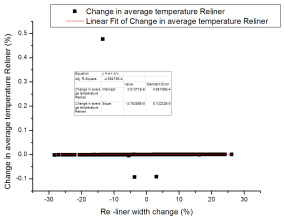

(m) Reliner width vs $T_{avg,Reliner}$
slope = -3.75E-5

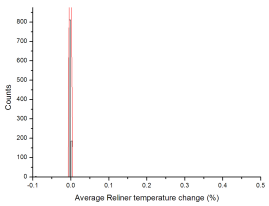

(n) Distribution of $T_{avg,Reliner}$
σ = 1.38E-3%

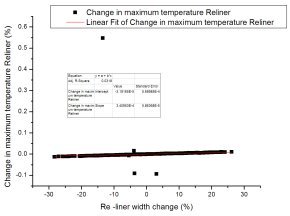

(o) Reliner width vs $T_{max,Reliner}$
slope = 3.41E-4

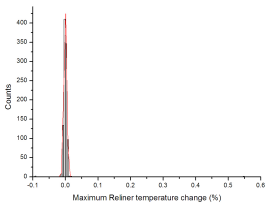

(p) Distribution of $T_{max,Reliner}$
σ = 4.51E-3%

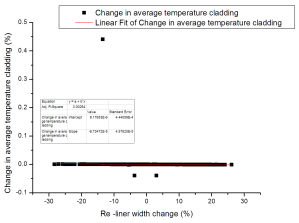

(q) Reliner width vs $T_{avg,cladding}$
slope = -8.73E-5

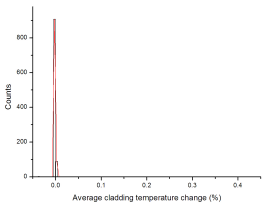

(r) Distribution of $T_{avg,cladding}$
σ = 1.23E-3%

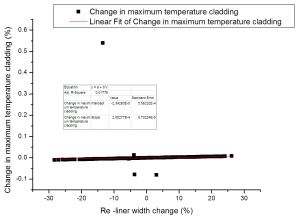

(s) Reliner width vs $T_{max,cladding}$
slope = 2.50E-4

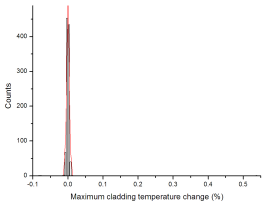

(t) Distribution of $T_{max,cladding}$
σ = 3.45E-3%

Figure B.3: Correlation between Re liner width perturbed and thermal parameters

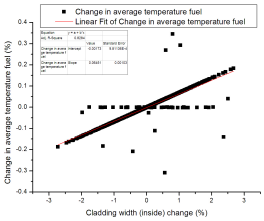

(a) Cladding width vs $T_{avg,fuel}$
slope = 0.06451

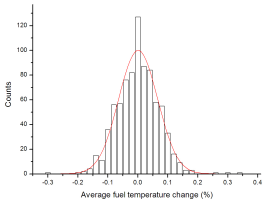

(b) Distribution of $T_{avg,fuel}$
$\sigma = 0.06497\%$

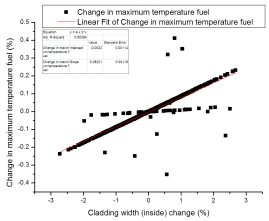

(c) Cladding width vs $T_{max,fuel}$
slope = 0.08221

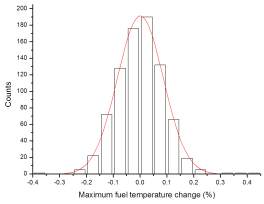

(d) Distribution of $T_{max,fuel}$
$\sigma = 0.08583\%$

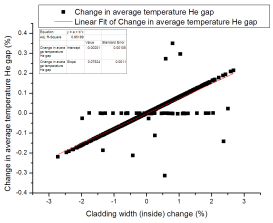

(e) Cladding width vs $T_{avg,Hegap}$
slope = 0.07524

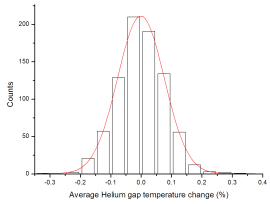

(f) Distribution of $T_{avg,Hegap}$
$\sigma = 0.07682\%$

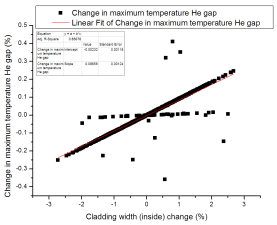

(g) Cladding width vs $T_{max,Hegap}$
slope = 0.08659

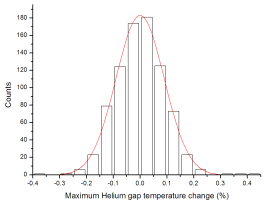

(h) Distribution of $T_{max,Hegapl}$
$\sigma = 0.08986\%$

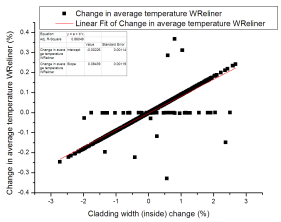

(i) Cladding width vs $T_{avg,WReliner}$
slope = 0.08439

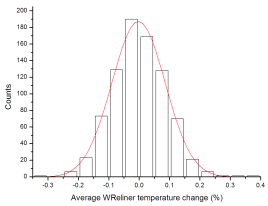

(j) Distribution of $T_{avg,WReliner}$
$\sigma = 0.08789\%$

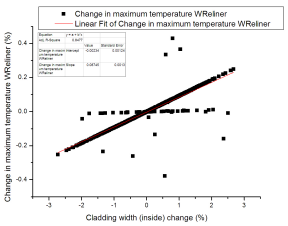

(k) Cladding width vs $T_{max,WReliner}$
slope = 0.08745

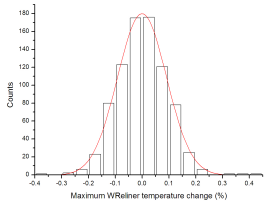

(l) Distribution of $T_{max,WReliner}$
$\sigma = 0.09151\%$

Figure B.4: Correlation between cladding width perturbed (inside) and thermal parameters

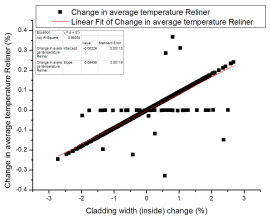

(m) Cladding width vs $T_{avg,Reliner}$
slope = 0.08436

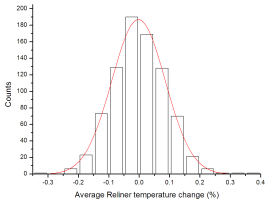

(n) Distribution of $T_{avg,Reliner}$
$\sigma = 0.08789\%$

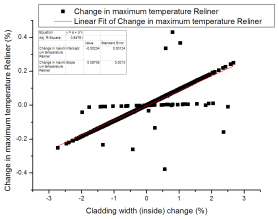

(o) Cladding width vs $T_{max,Reliner}$
slope = 0.08736

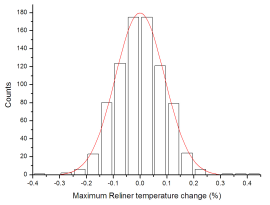

(p) Distribution of $T_{max,Reliner}$
$\sigma = 0.09175\%$

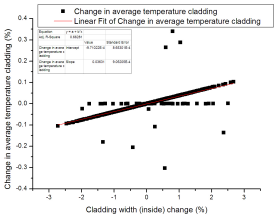

(q) Cladding width vs $T_{avg,cladding}$
slope = 0.03631

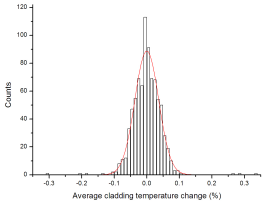

(r) Distribution of $T_{avg,cladding}$
$\sigma = 0.03649\%$

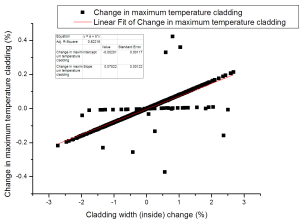

(s) Cladding width vs $T_{max,cladding}$
slope = 0.07522

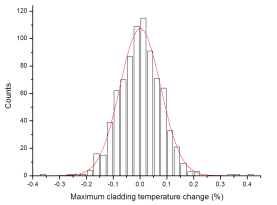

(t) Distribution of $T_{max,cladding}$
$\sigma = 0.07571\%$

Figure B.4: Correlation between cladding width perturbed (inside) and thermal parameters

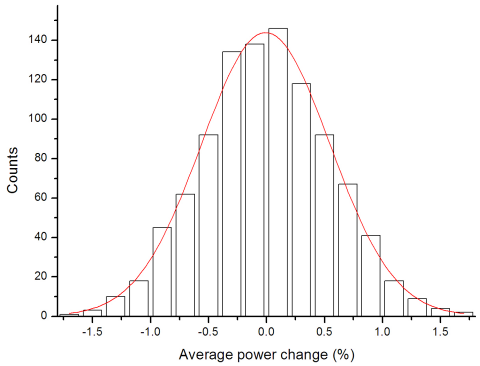

(a) Distribution of P_{avg}
$\sigma = 0.55381\%$

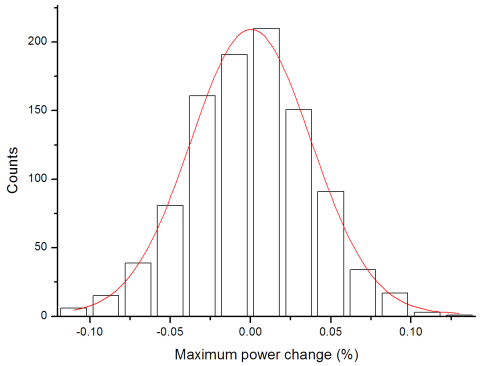

(b) Distribution of P_{max}
$\sigma = 0.03756\%$

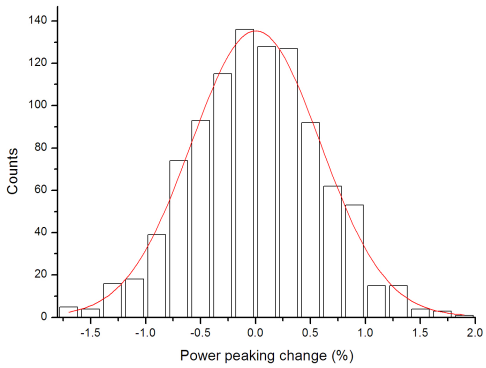

(c) Distribution of power peaking
$\sigma = 0.58745\%$

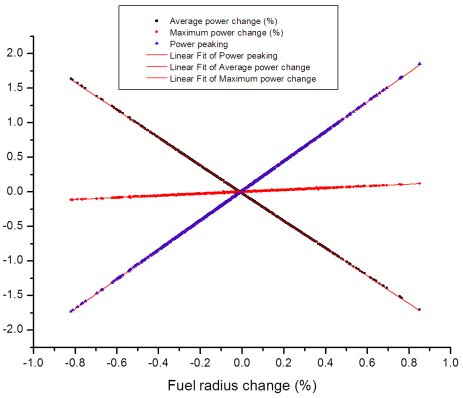

(d) Fuel pellet radius vs diverse parameters

Figure B.5: Correlation between fuel pellet radius perturbed and power density parameters

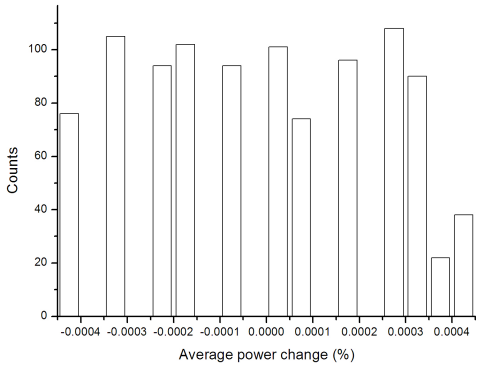

(a) Distribution of P_{avg}
σ non existent

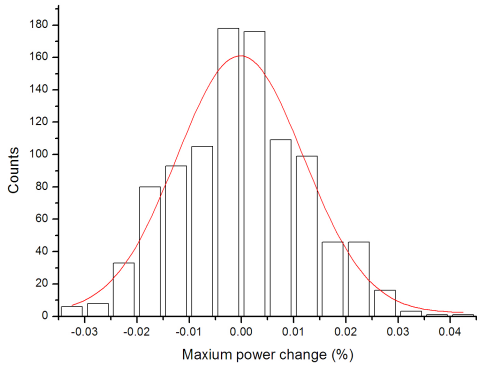

(b) Distribution of P_{max}
$\sigma = 0.01213\%$

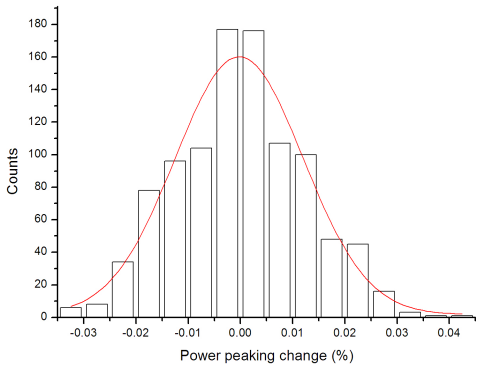

(c) Distribution of power peaking
$\sigma = 0.01227\%$

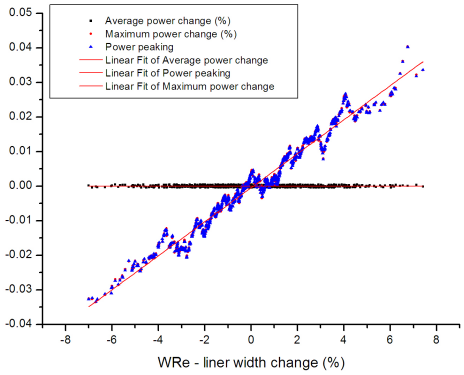

(d) WReliner width vs diverse parameters

Figure B.6: Correlation between WRe liner width perturbed and power density parameters

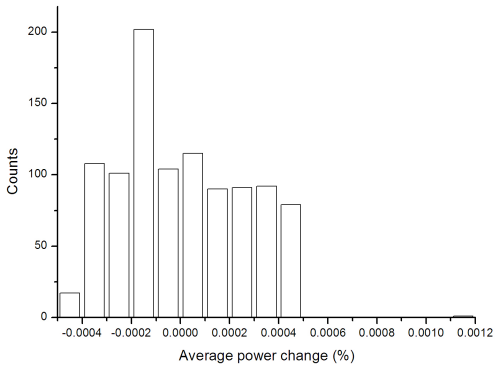

(a) Distribution of P_{avg}
σ non existent

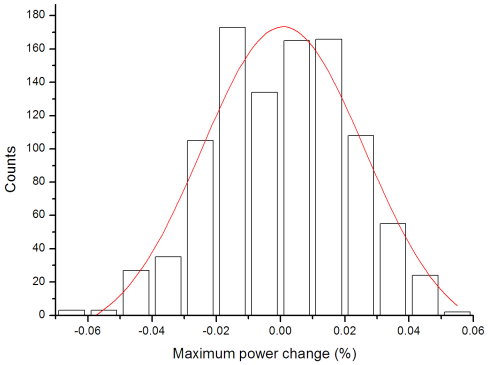

(b) Distribution of P_{max}
$\sigma = 0.02531\%$

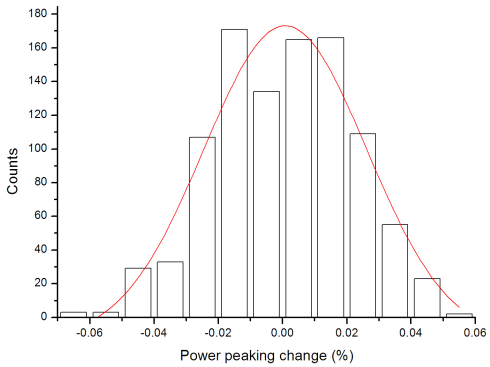

(c) Distribution of power peaking
$\sigma = 0.2034\%$

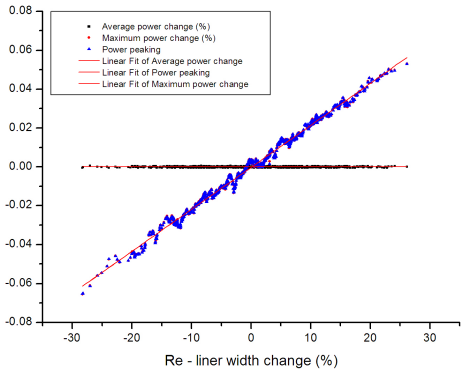

(d) Re liner width vs diverse parameters

Figure B.7: Correlation between Re liner width perturbed and power density parameters

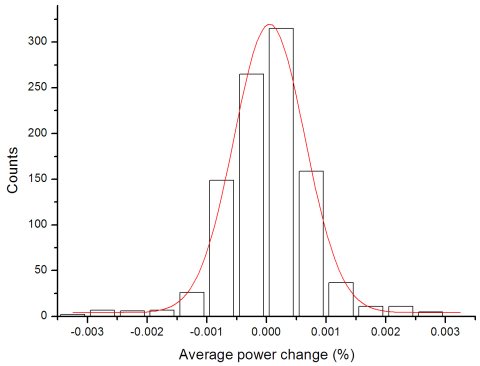

(a) Distribution of P_{avg}
$\sigma = 0.00060\%$

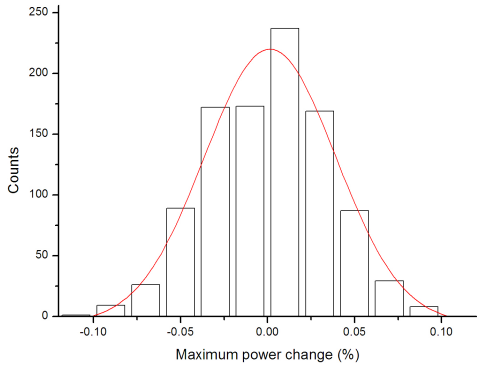

(b) Distribution of P_{max}
$\sigma = 0.03780\%$

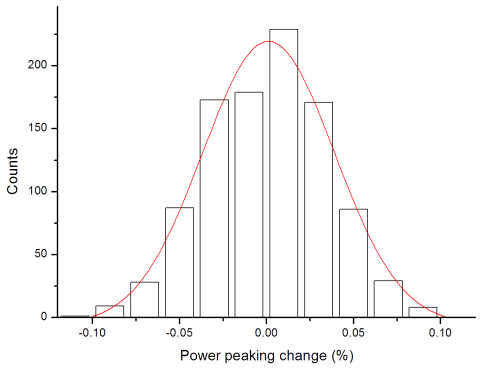

(c) Distribution of power peaking
$\sigma = 0.03792\%$

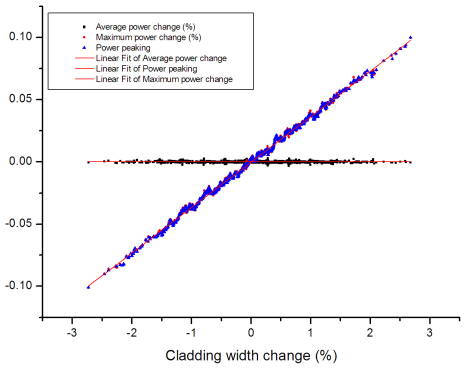

(d) Cladding width vs diverse parameters

Figure B.8: Correlation between cladding width perturbed (inside) and power density parameters